University of Nevada
Reno

Ultrasensitive Force Sensing with Nanospheres in an Optical Standing Wave Trap

A thesis submitted in partial fulfillment of the
requirements for the degree of Master of Science
in Physics

by

Mark S. Cunningham

Dr. Andrew A. Geraci, Thesis Advisor

December 2017

THE GRADUATE SCHOOL

We recommend that the thesis
prepared under our supervision by

MARK CUNNINGHAM

Entitled

Ultrasensitive Force Sensing with Nanospheres in an Optical Standing Wave Trap

be accepted in partial fulfillment of the
requirements for the degree of

MASTER OF SCIENCE

Andrew A. Geraci, Ph.D., Advisor

Jonathan Weinstein, Ph.D., Committee Member

Siddhartha Pathak, Ph.D., Graduate School Representative

David W. Zeh, Ph.D., Dean, Graduate School

December, 2017

Abstract

This thesis details the experimental progress developing a state-of-the-art neutral force sensor using an optically levitated nano-sphere. Trapping 300 nm diameter fused silica spheres using a dual beam optical standing wave trap, we have experimentally reported a force sensitivity of 1.63 $\pm 0.37 \mathrm{aN/Hz}^{1/2}$. Also we have measured the heating rate of the nano-spheres at high vacuum, and we have experimentally explored the nano-sphere dynamics to optimize the trap stability at pressures on the order of 10^{-6} mbar. At this pressure, with averaging times on the order of 10^5 s, we have demonstrated force sensing at 5.8 ± 1.3 zN.

The experimental merit of this ultra-sensitive neutral force sensor is to test for non-Newtonian gravity-like forces on the micron scale. In order to push our sensitivities even further toward this goal, we have developed a second optical standing wave trap system. Using two laser frequencies, 1596 nm and 1064 nm, incident on a single hemispherical optical cavity, we have successfully trapped nano-spheres inside the optical standing wave trap. In this thesis we outline the frequency stabilization system, the optical cavity, and experimental progress in overlapping both optical standing wave traps. We will outline further improvements that can and are being made to improve the system. Also included is an outline of our data analysis using Matlab to show nano-sphere displacement and force measurement.

Acknowledgments

I would like to thank my PhD advisor, Dr. Andrew Geraci, for his advice, encouragement, feedback, and time. Additional thanks go to my committee members, Dr. Jonathan Weinstein and Siddhartha Pathak, for their expertise and valuable perspective.

Many thanks to Dr. Gambhir Ranjit for his hard work, outstanding mentorship, and invaluable friendship. Additional thanks to the staff of the UNR Physics machine shop, Wade Cline and Carl Davidson, for their assistance and experimental expertise. Also every member of Dr. Geraci's research group, past and present.

To the UNR Physics Department, especially the office staff, for guidance and logistical support.

Finally, to my wife, Sara, for her help is proofreading the manuscript and her love, support, and understanding through all of my academic career.

This work is funded by National Science Foundation grants # NSF PHY-1205994, # NSF PHY-1506431, and the Heising-Simons Foundation

Contents

List of Figures

Chapter 1

Introduction

Shortly after the advent of lasers, early experiments were performed in the realm of trapping small particles with light. The first experiments of this type were done with small particles and tightly focused beams[1][2]. Decades later, that work was the foundation of laser trapping, cooling ensembles of atoms[3][4][5], optical tweezers[6], and biophysics research[7][8]. Improvements in cooling these atomic ensembles gave rise to the rich physics of degenerate gasses. But, in recent years, there has been a return to using mesoscopic systems with optically levitated spheres to explore new physics. In essence viewing the quantum nature of the world with new light using micro-spheres and nano-spheres.

1.1 History and Theory

In 1619, Johannes Kepler observed that the curve of the tail of a comet always points away from the sun. His explanation was the concept of radiation pressure. As light interacts with physical particles, it imparts momentum.

Later, Maxwell's theory of electromagnetism expresses absorbed radiation pressure as the energy flux using the time average of the Poynting vector, $\mathbf{S} = \mathbf{E} \times \mathbf{H}$, divided by the speed of light. Here $\mathbf{E}$ is the Electric field and $\mathbf{H}$ is the magnetizing field.

The pioneering work using optically levitated silica micro-spheres was reported by Ashkin in the early 1970s[1][2]. Using focused lasers and low absorption particles, he was able to trap and accelerate particles using the radiation pressure of light.

1.1.1 Arthur Ashkin's Pioneering Work

In figure 1.1 one can see the illustration of his initial experiments in accelerating and trapping silica micro-spheres. As shown in figure 1.1a, Ashkin focused down an Argon laser at 514.5 nm to a beam diameter of $2w_0$ equal to 12.4 μm into a glass cell of thickness $t = 120\,\mu$m. Inside the glass cell there are three sizes of micro-spheres: 0.59 μm, 1.31 μm, and 2.68 μm inside a water solution. If any of the spheres come into contact with the laser light they are simultaneously accelerated into the side of the glass cell and drawn into the axis of the laser beam until they are pinned on the side of the cell in the center of the laser beam. The micro-spheres are not stuck to the side of the wall as we see in the details of the second trap configuration shown in figure 1.1b.

This second configuration has one added antiparallel beam, which focuses just before the focus of the couterpropagating beam, trapping the micro-sphere between the two foci of the beams. Here the 2.68 μm diameter micro-spheres are used in an open cell filled with water. The spheres first interact with a single beam, similar to figure 1.1a, which accelerates the micro-sphere till it is pinned against the wall. Then the second beam is turned on, loading the trapped sphere into the optical potential well in the center of the two foci. This trap is acheived with 128 mW of power in each beam[1]. In later work, Ashkin reported the trapping of micro-spheres with a 20 μm diameter to pressures of $\sim 10^{-6}$ Torr[9].

1.1.2 Radiation Pressure

In his explanation of how the spheres are trapped one can gain a physical understanding by looking at the simple ray optics in figure 1.2. A Gaussian beam with the transverse electromagnetic mode (TEM) of 00 is incident on a highly transparent sphere. By tracing the rays of the sphere, one can understand the forces experienced by the micro-sphere. Noting the propagation direction of the light and conservation

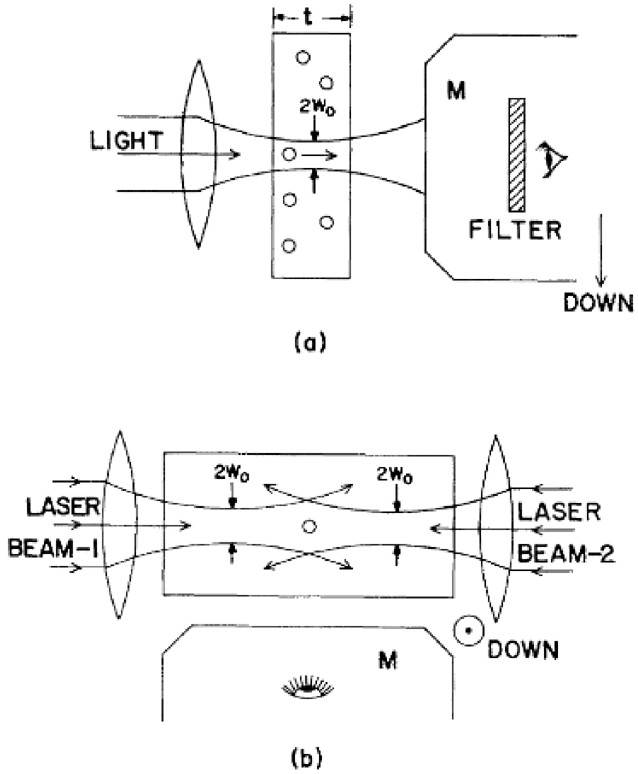

Figure 1.1: a)Schematic shown for the initial silica accelerating experiment performed by Ashkin. b)By adding a second beam Ashkin was able to trap a microsphere using only the radiation pressure of light; figure from reference[1].

of momentum, we see the acceleration of the micro-sphere in the direction of light's Poynting vector and toward the most intense part of the beam i.e. the center of the Gaussian beam or the beam axis.

As the application of Ashkin's work shifted to atoms[5] and biological observation and manipulation[7][8], the work with highly transparent micro-spheres had to wait for decades before those ideas sparked development for the application of quantum mesoscopic systems.

1.2 Current Research of Levitated Spheres

Recent advancements in optically levitated nanosphere systems have led to working toward ground state cooling[11][12][13][14]. In efforts to acheive the ground

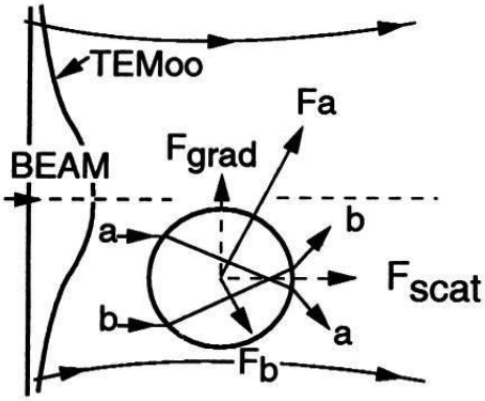

Figure 1.2: An off-axis micro-sphere will have more photons travel the path of the ray trace labeled 'a', therefore the force in the F_a direction is greater than that in the F_b direction. In the transverse direction to the beams propagation, the gradient force, F_{grad}, draws the micro-sphere toward the center of the axis shown by the dotted line. The axial force of F_a and F_b add together to give the scattering force, F_{scat}, in the direction of laser's propagation. This figure is from reference[10].

state a variety of cooling techniques have been used, including parametric feedback cooling[15][16], active feedback cooling[14], cavity cooling[11][17][13], and sympathetic cooling[18]. Reaching the ground state in a nano-sphere experimental platform has potential in matter wave interferometry[19][20] , quantum tests in mesoscopic systems[11][21][22], and quantum optomechanics in hybrid systems[18]. Other applications of optically levitated nano-spheres include quantum information[11][21], gravitational wave detection[23], inertial sensing[24], Brownian motion[25], Casimir force tests, and gravitational inverse square law violations[26]. In figure 1.3 there is a review of some of the research groups around the world and their various optically levitated nano-sphere systems. Experimentally the field is currently exploring these mesoscopic systems through controlling the charge present on the nano-spheres[27], using hybrid traps involving cavities and ion traps[13][28], controlling the motion control over large distances[29][30], and using these systems to model stochastic bistable dynamics[31], the realization of thermal squeezed states[32], levitated nano-diamonds with NV centers[33][34], and coherent control[35].

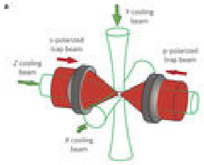

Mark Raizen Group
Center for Nonlinear Dynamics and Department of Physics,
The University of Texas at Austin, Austin, Texas 78712, USA
Using 1064 nm dual beam dipole trap with active feedback
beams at 532 nm.
Experiments is cooling[**14**], brownian motion[25].

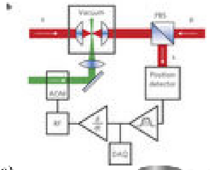

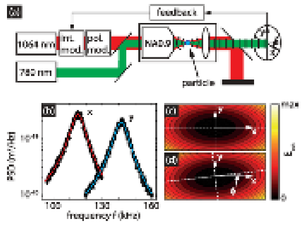

Novotny Group
Photonics Laboratory, ETH Zürich, CH-8093 Zürich, Switzerlanda
Using a 1064 nm laser to trap 136 nm diameter spheres.
Imaging with a 780 nm laser and feedback cooling employed.
Experiments in coherent control cooling [**35**],
controlling charge [27], and photon recoil measurement[12].

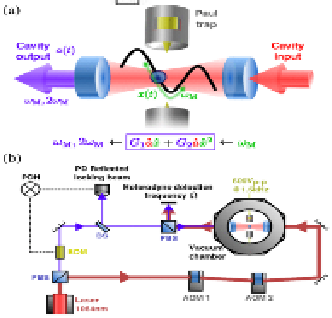

Barker Group
Department of Physics and Astronomy, University College
London, Gower Street, London WC1E 6BT, United Kingdom
Using a paul trap and cavity cooling and trapping laser at
1064 nm demonstrates cavity cooling of a charged
nano-sphere of 209 nm.
Experiments in hybrid paul trap/cavity cooling [13,**28**].

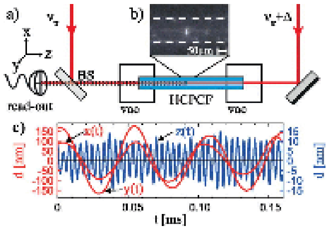

Aspelmayer Group
Vienna Center for Quantum Science and Technology (VCQ),
Faculty of Physics, University of Vienna,
A-1090 Vienna, Austria
A 387 nm diameter silica particle trapped in a hollow core
photonic crystal fiber using counter propagating
1064 nm lasers.
Experiments in cooling and motion controll[**29**], cavity
cooling[17].

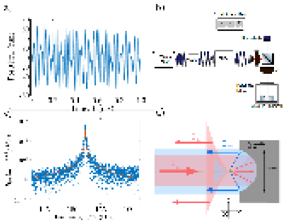

Ulbricht Group
Department of Physics and Astronomy, University of
Southampton, SO17 1BJ, United Kingdom
Using a parabolic mirror trap and a 1550 nm trapping
laser to optically trap and levitate 26 - 160 nm particles.
Experiments in thermal squeezed states [32], cooling [**16**].

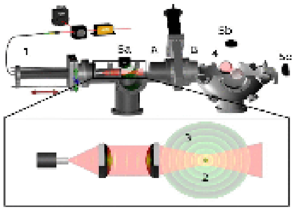

Quidant Group
ICFO-Institut de Ciencies Fotoniques, The Barcelona Institute
of Science and Technology, 08860 Castelldefels (Barcelona),
Spain
Using 1064 nm fiber optical tweezer and optical cavity to trap
and manipulate a particle of ∼ 75 nm radius.
Experiments in motion control and cooling[**30**], modeling
stochastic bistable dynamics[31].

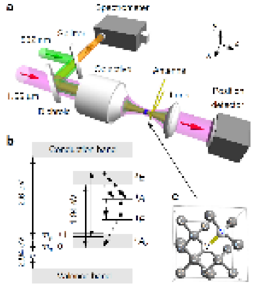

Li Group
Department of Physics and Astronomy, Purdue University,
West Lafayette, Indiana 47907, USA.
Using 1550 nm optical tweezer to levitate nano-diamonds
with NV centers with 100 nm diameter.
Experiments in spin control[**34**].

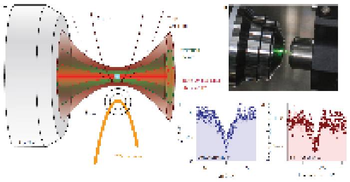

Vamivakas Group
Center for Coherence and Quantum Optics, University
of Rochester, Rochester, New York 14627, USA.
Levitation of 40 nm nano-diamonds using optical
tweezer at 1064 nm.
Experiments in single spin nano-diamonds [**33**].

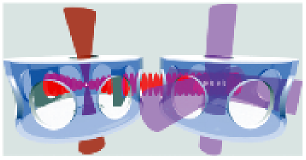

Geraci Group
Department of Physics, University of Nevada, Reno,
Reno, Nevada 89557, USA
Using spheres ranging from 170 nm - 3 micron diameters and
using 1596 nm, 1064 nm, and 780 nm lasers in dual beam,
cavity and optical tweezer traps.
Experiments in sympathetic cooling [**18**], and force sensing [42,43].

Figure 1.3: Overview of Groups working with optically levitated nano-spheres; figures reproduced from the bold cited references.

1.3 Force Sensing Application

In order to perform force tests of gravitational wave detection, Casimir forces, and gravitational inverse square law violations, an ultra-sensitive force sensor is required [26], which is precisely what we are developing using an optically levitated nanosphere. Because of the thermal noise limitations in state-of-the-art force sensors, such as nanotube mechanical resonators[36], microcantilevers[37], trampoline resonators [38], MEMS Sensors[39][40], and nanomembranes[41], they require operating in cryogenic environments to maximize force sensitivity. At room temperatures the best force sensitivities of those systems are on the order of ~ 10 aN/Hz$^{1/2}$.

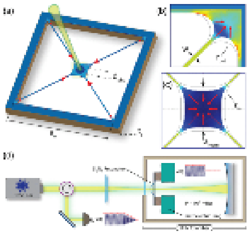

Groblacher Group
Kavli Institute of Nanoscience, Delft University of Technology, Lorentzweg 1,
2628CJ Delft, The Netherlands

Ultrathin Silicon Nitride membranes with a calculated sensitivity of 10 aN/Hz$^{1/2}$ at room temperature[41]

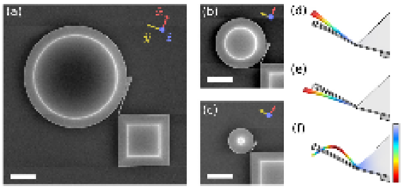

Davis Group
Department of Physics, University of Alberta, Edmonton, Alberta T6G
2E9, Canada

Nanomechanical cantilever demonstrating a force sensitivity of 132 aN/Hz$^{1/2}$ at room temperature[37]

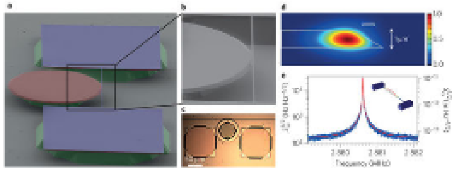

Kippenberg Group
Ecole Polytechnique Fédérale de Lausanne, EPFL, 1015 Lausanne,
Switzerland

Silicon Nitride nanomechanical beam coupled to Silicadisk demonstrating 74 aN/Hz$^{1/2}$ at room temperature [40]

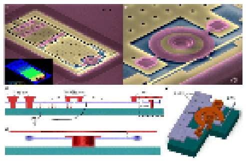

Aksyuk Group
Center for Nanoscale Science and Technology, National Institute of Standards
and Technology, 100 Bureau Dr, Gaithersburg, MD 20899, USA

Silicon Nitride MEMs sensor reporting 53 aN/Hz$^{1/2}$ at room temperature[39]

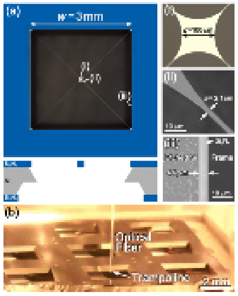

Sankey Group
Department of Physics, McGill University, Montréal, Québec, H3A 2T8,
Canada

Silicon Nitride "Trampoline" exhibiting 20 aN/Hz$^{1/2}$ sensitivity at room temperature [38]

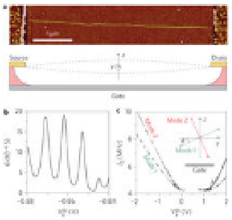

Bachtold Group
ICFO-Institut de Ciencies Fotoniques, Mediterranean Technology Park,
08860 Castelldefels (Barcelona), Spain

Carbon nanotube resonator cooled to 1.2 K exhibits a sensitivity of 12 zN/Hz$^{1/2}$ [36]

Figure 1.4: General Overview of Current Force Sensing Research; images reproduced from the cited references.

We believe that optically levitated nano-spheres are ideal for the application of precision force sensors. A nano-sphere that is optically levitated experiences minimal friction and is decoupled from the environment resulting in better sensitivities at room temperature. We have demonstrated sensitivities at ~ 1 aN/Hz$^{1/2}$ with cooling of the center-of-mass motion to $\sim$400 mK at a pressure of 5×10^{-6} Torr. We have also shown that 300 nm optically levitated nano-spheres with long averaging times can be used as calibrated zeptonewton force sensors while in a standing wave optical trap. A standing wave optical trap is a series of optical potential wells along the laser beam path that are created by constructive and destructive interference of interacting electric fields. With the addition of a hemispherical cavity and cavity assisted cooling this system is a promising configuration for measuring neutral forces near surfaces. As we move toward a dual optical trapping system of an optical cavity and a dual beam standing wave we expect to push our system's sensitivity by 1-2 orders of magnitude. Also cavity cooling could assist us in achieving even lower center-of-mass motion temperatures.

1.4 Our Levitating Micro/Nano-sphere Systems

In our lab we have experimented with four sizes of optically levitated spheres spanning in size from 3 μm to 170 nm diameters. In this thesis we will primarily discuss the work done with 300 nm diameter nano-spheres[42] with some reference to earlier work with 3 μm micro-spheres[43]. Following is an image of an optically levitated 3 μm micro-sphere.

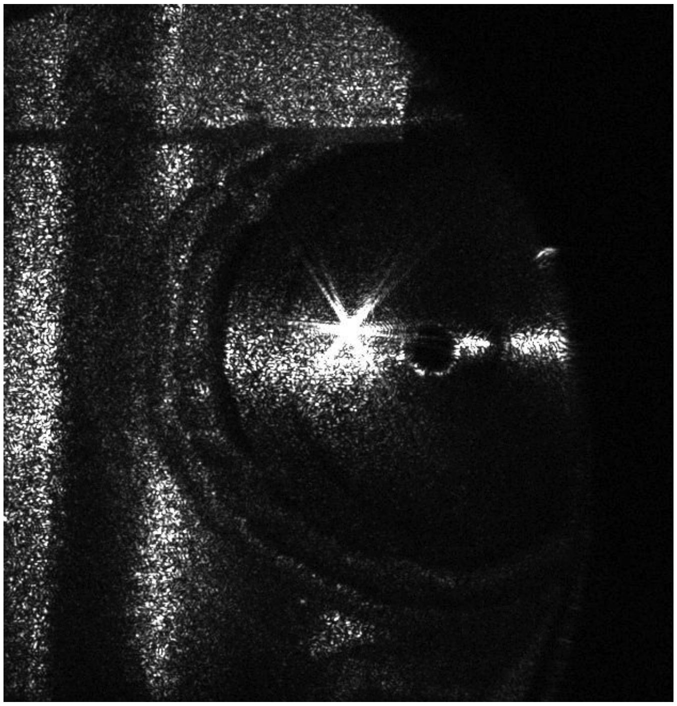

Figure 1.5: Picture of a 3 μm diameter micro-sphere optically levitated using a 1064 nm dual beam dipole trap. The bright spot in the middle of the image is light from the trapping laser that is scattered by the micro-sphere.

The micro-sphere in figure 1.5 is being optically levitated using a dual beam optical dipole trap. As we transition to smaller nano-spheres the size of the sphere will now be smaller compared to the optical standing wave trap site's separation defined by $\lambda/2$ of the trapping laser. But like the earlier work in our lab the initial work with optically levitated spheres was done with larger silica micro-spheres where the standing wave's gradients were averaged over the size of the micro-sphere.

After the nano-sphere is loaded into the trap, if we can move the nano-sphere to a trap site near a thin flat gold mirror in our experimental setup, then we can perform fundamental tests of physics in the area of Deviation from Newtonian Gravity along with Casimir force test measurements[26].

1.5 Search for Deviation from Newtonian Gravity

The force felt between two objects can be expressed as $F = \frac{Gm_1m_2}{r^2}$ where F is the force, G is the gravitational constant, m_1 and m_2 are the respective masses, and r is the distance between the two objects. The equation has been tested and tried with large objects, but because of the relative strength of gravity compared to other fundamental forces in the standard model known as the hierarchy problem, there are theories beyond the standard model which predict a deviation of Newtonian gravity at short ranges[44][45].

This deviation is characterized by the yukawa potential:

$$U = \frac{Gm_1m_2}{r}\left(1 + \alpha e^{-r/\lambda}\right) \tag{1.1}$$

where α is the strength of the interaction and λ is the interaction length[26].

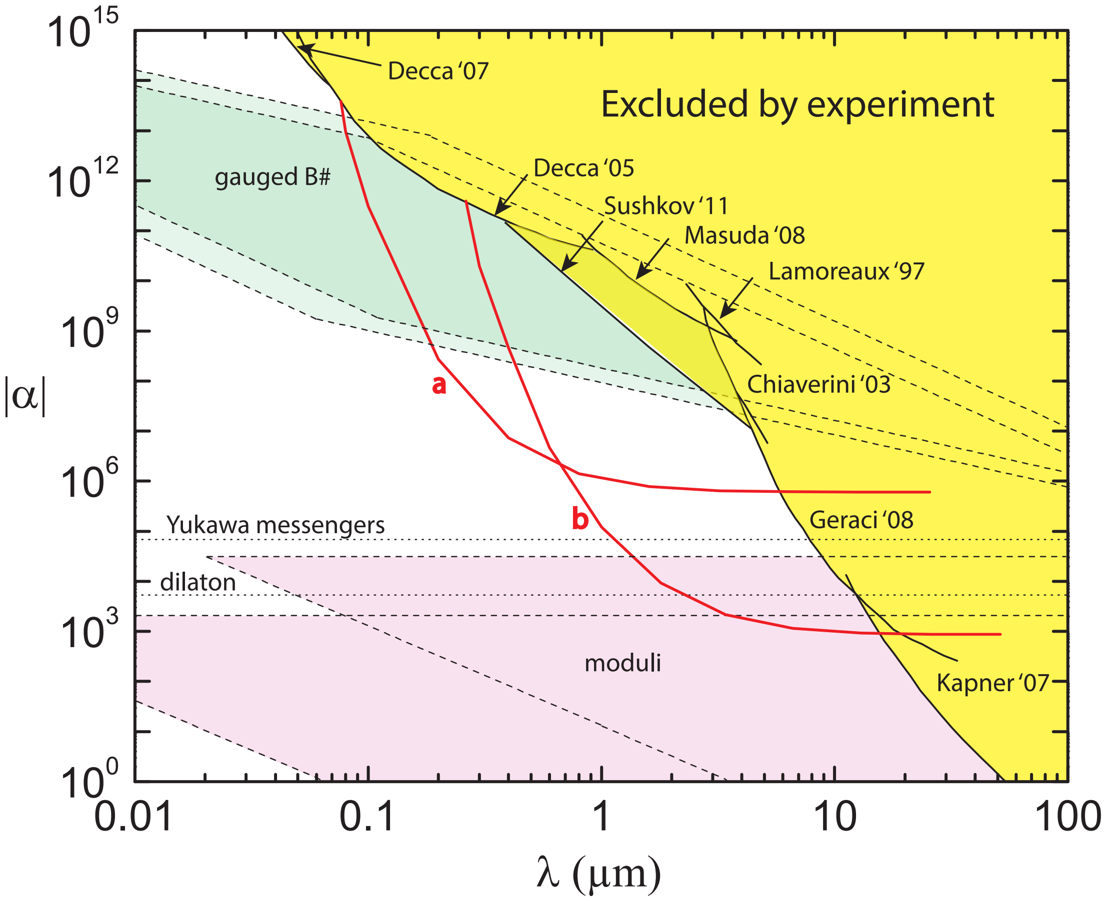

Figure 1.6: Phase Space Plot for the Non-Newtonian gravitational like Forces: the two axes correspond to the two parameters in the yukawa potential characterizing the correction $U = \frac{Gm_1m_2}{r}\left(1 + \alpha e^{-r/\lambda}\right)$. Curve 'a' is for a 300 nm diameter nano-sphere where curve 'b' is for a 3 μm diameter micro-sphere; figure adapted from reference[26] .

The past explorations to search for non-Newtonian gravity-like forces on the micron scale were performed with torsion pendulums[46][47], torsion balances[48][49], and micro-mechanical oscillators[50][51][52][53]. Our proposed system as shown in figure 1.7 can be used to explore the parameter space carved by the two red curves in figure 1.6; curve 'a' is for a 300 nm diameter nano-sphere where curve 'b' is for a 3 μm diameter micro-sphere.

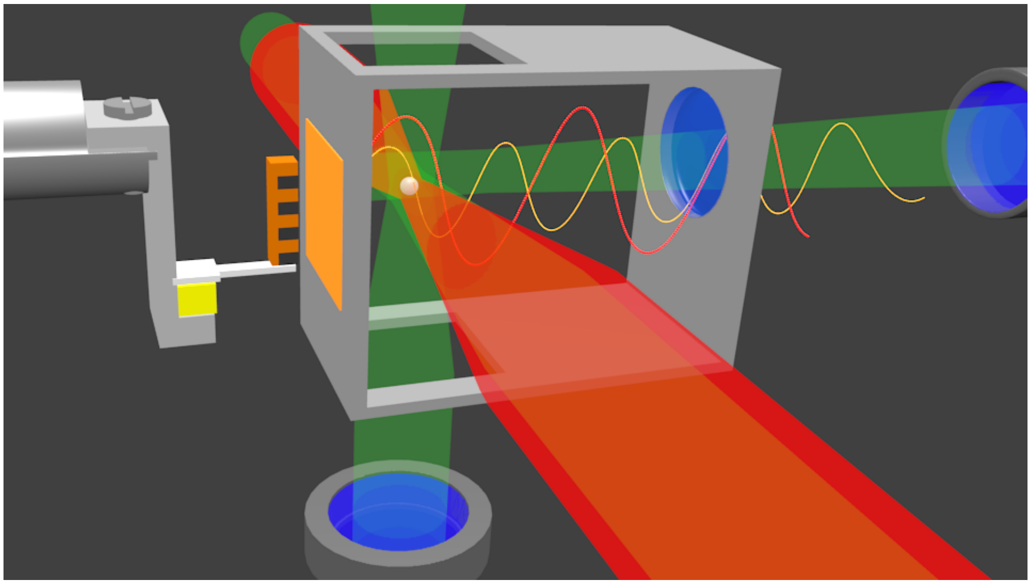

Figure 1.7: The Optically Levitated Nano-Sphere Force Sensor: a combined cavity-dual beam standing wave system of an optical cavity and a dual beam standing wave trap. Inside the cavity there is an optical trap (red sinusoid at 1596 nm) and cooling beam (yellow sinusoid at 1064 nm). The nano-sphere is loaded into the dipole trap (red) with 3 dimensional active feedback cooling beams (green). Behind the thin gold mirror, near the nano-sphere, there is an oscillating mass on the end of a cantilever; the mass consists of alternating materials, gold and silicon.

The dual beam optical standing wave trap consists of two dipole beams with offset foci between 50 - 100μm apart, shown in figure 1.7 in red. Also shown are three cooling beams in green. Finally we have two beams, one trapping and one cooling/readout, incident to a hemispherical experiment cavity consisting of a flat gold mirror. Using a reference cavity we stabilize the laser frequency of both beams incident to the experimental cavity as well as the length of the experimental cavity. The nano-sphere is loaded into the dual beam optical standing wave trap. Which, with the help of active feedback cooling, stabilizes the nano-sphere's motion in the transition from low to high vacuum. In the cavity itself, an optical lattice can confine nano-spheres near the surface of the flat square gold mirror shown above. The imaging is done with two quandrant photodectors (QPD) and high numerical aperture (NA) lenses collecting scattered light from the nano-sphere and the reflected cavity readout in the cooling beam. The optical cooling consists of two cooling schemes: active feedback cooling in three dimensions (green) and cavity assisted cooling (yellow sinusoid). The details of this system will be discussed further in the following chapters.

Chapter 2

Experimental Setup

Our current experimental setup consists of two types of optical traps: a dual beam dipole standing wave trap, and an optical standing wave trap inside an optical cavity. We have previously shown zeptonewton force sensitivities over long averaging times in our dual beam optical standing wave dipole trap[42]. To ultimately measure forces at a short interaction range in our search for non-Newtonian gravity-like forces, we are transitioning to an optical cavity standing wave. Currently to measure the forces exerted on a levitated nano-sphere we employ two quadrant photodetectors (QPD) to measure position. From the displacement spectra we can deduce forces exerted onto the nano-sphere. We make those deductions by calibrating the motion of the nano-sphere using the fact that the nano-spheres are sometimes charged or are subject to a known optical lattice spacing.

2.1 Dual Beam Dipole Standing Wave Trap

The Dual Beam Dipole Standing Wave Trap is created by using a 3 W, 1064 nm wavelength Nd:Yag Laser[54]. The beam is magnified to 9 mm and collimated using a telescope composed of a 30 mm focal length planoconvex lens with a 125 mm focal length acromat. The beam then passes through a $\lambda/2$ waveplate into a polarizing beam cube, where the beam is split into its respective polarizations. The $\lambda/2$ waveplate is used to balance the power between the S and P polarized beams. After passing through the polarized beam cube, the two laser paths are directed to periscopes opposite of each other and then focused through two 50 mm focal length[55] lenses with the foci offset by 50-100 μm. Here, the focus of the beam is before the counter propagating beam's focus; this configuration creates a stable optical trap.

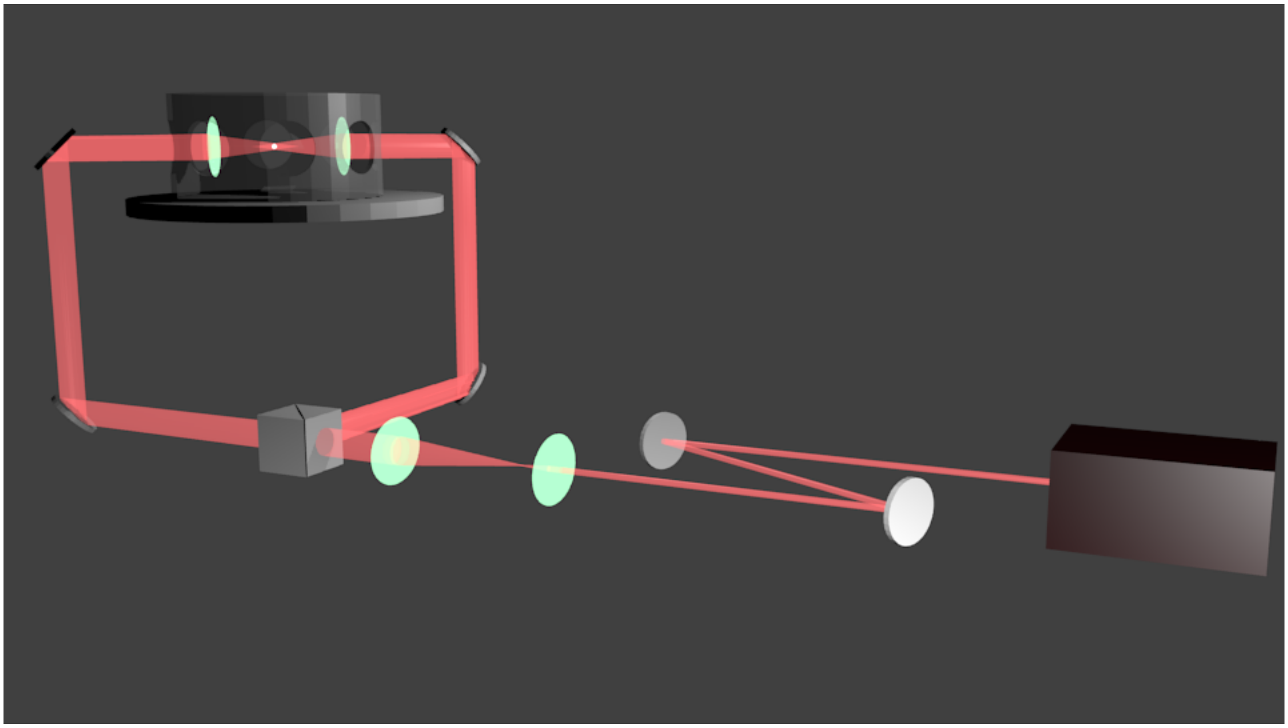

Figure 2.1: A graphical representation of the optical standing wave trap. The beam is expanded in the first telescope indicated by the two lenses in blue-green. Then, the S and P polarization are split by the polarizing beam cube. The beam travels to two periscopes opposite of each other and then the beams are focused 50-100 μm in the center creating the optical standing wave trap discussed in the text.

The imperfection in the polarizing beam cube causes a small percent of the P polarized light to travel in the S polarized light's beam path. The constructive interference causes a slight optical standing wave as seen in figure 2.2. A simulated 0.01% of the P polarization electric field results in a 0.2% intensity modulation in the optical standing wave.

In this simulation the electric field is given by

$$E = E_0\, e^{i(k\mathbf{z}-\omega t)} \tag{2.1}$$

where k is the wavenumber, $\mathbf{z}$ is the position, ω is the angular frequency, and t

is time. The actual electric field is the real part of E, complex notation is used here as a mathematically efficient way to calculate interference. E_0 is defined as:

$$E_0 = \sqrt{\frac{4\,P}{\epsilon_0\, c\, \pi\, w(z)^2}} \tag{2.2}$$

Here P is the laser power, ϵ_0 is the permittivity of free space, c is the speed of light, and $w(z) = w_0\sqrt{1 + (\frac{z}{z_r})^2}$ is the $1/e^2$ radius of the laser beam dependent on the distance from the focus (z), w_0 is the beam waist, and the Rayleigh range is defined as $z_r = \frac{\pi w_0^2}{\lambda}$.

After adding the electric fields of the S polarized light and the P polarized light we can model the extent of interference between the two beams. We use the total electric field to calculate the intensity of the laser light in the standing wave optical trap between the foci of the two counter propagating beams using $I = \frac{\epsilon_0\, c}{2}\, E^2$. From the intensity of the lasers, we can calculate the effective force applied to the nano-sphere, by adding the scattering force, F_{scat}, and gradient force, F_{grad}. The scattering force is in the direction of the laser propagation, $\hat{z}$, and is given by:

$$\vec{F}_{scat} = \frac{128\,\pi^5\, r^6}{3\, c\,\lambda^4}\left(\frac{\epsilon^2 - 1}{\epsilon^2 + 2}\right)^2 I\,\hat{z}\,[56] \tag{2.3}$$

The gradient force is shown here:

$$\vec{F}_{grad} = \frac{2\pi r^3}{c}\left(\frac{\epsilon^2 - 1}{\epsilon^2 + 2}\right)^2 \vec{\nabla} I\,[56] \tag{2.4}$$

When all the forces are added together,$F_{eff} = F_{scat} + F_{grad}$, one can look at the axial component of the force. Figure 2.2 shows the total axial force experienced by the nano-sphere based on its position in space.

This resulting modulation predicts multiple possible trapping sites in between the two foci, the spacing between two adjacent sites is set by $\lambda/2$, where λ is the wavelength of the trapping laser(1596 nm). As one can see in the contour plot in

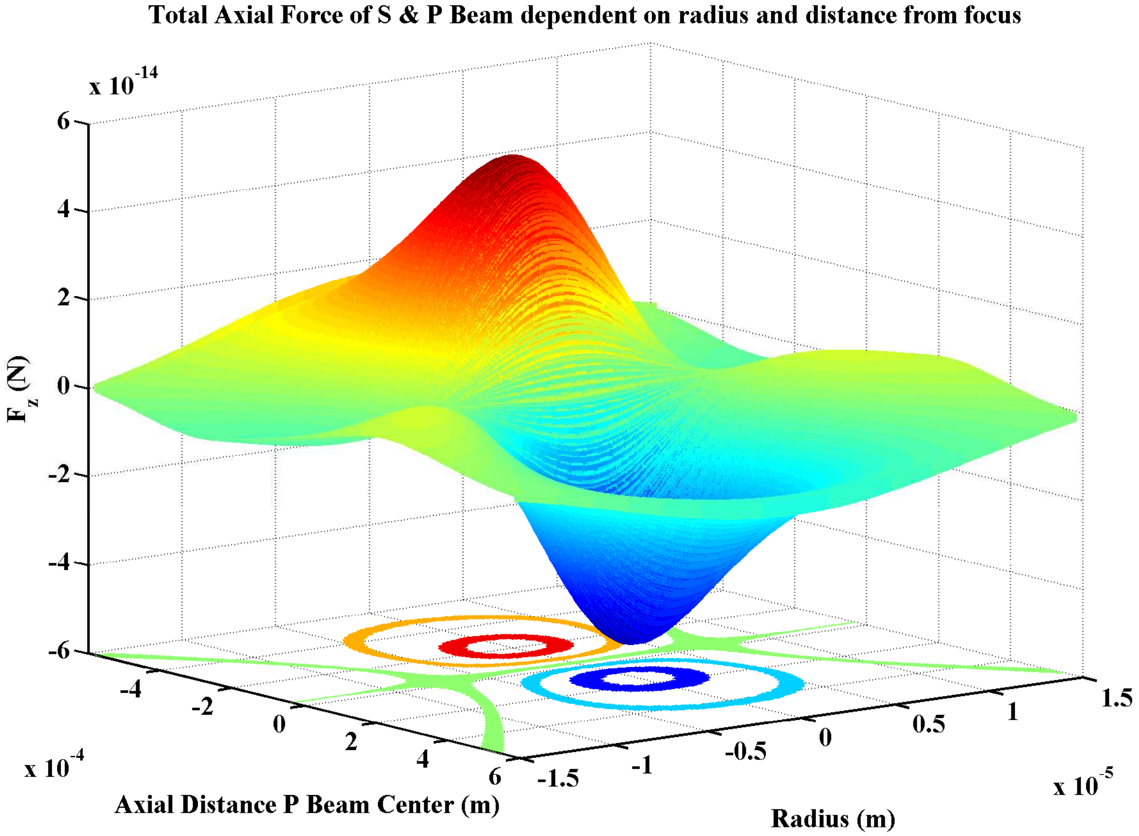

Figure 2.2: This is the total axial force experience by a nano-sphere in the optical standing wave trap. The model is done for a nano-sphere of 300 nm diameter with a density of 2200 kg/m^3. The optical standing wave is composed of 1.1 W of power split between the two counter propagating beam corresponding to approximately 60% of the maximum driving current on the Nd:YAG laser[54] at 1064 nm wavelength. The two counter propagating beams are focused down to 8 μm beam waists to create the optical standing wave trap. The x axis is the distance from the focus of the P polarized beam and the y axis corresponds to the position of a sphere from the center of the two Gaussian beams. This model assumes Gaussian beams are aligned perfectly antiparalell to each other. The P polarization that follows the S polarized beam path is about 0.01% of the total P polarized laser light giving way to interference of 0.2% intensity modulation in the optical standing wave.

figure 2.2 the thick green area is where the nano-sphere experiences zero force axially indicating multiple positions of the trapping sites. In order to resolve the multiple sites, one can zoom in to reveal the optical standing wave trap spacing, corresponding to $\lambda/2$. To see the spacing better figure 2.3 is a plot of the on axis axial force with a zoomed in span of 10 μm around the center of the foci offset showing the multiple possible trapping sites in the upper right hand corner. Also shown in green in figure 2.3 is a non-interfering force, or the force in the absence of an optical standing wave. Here the crossing at zero occurs when the scattering force of the two counter propagating beams is equal and opposite.

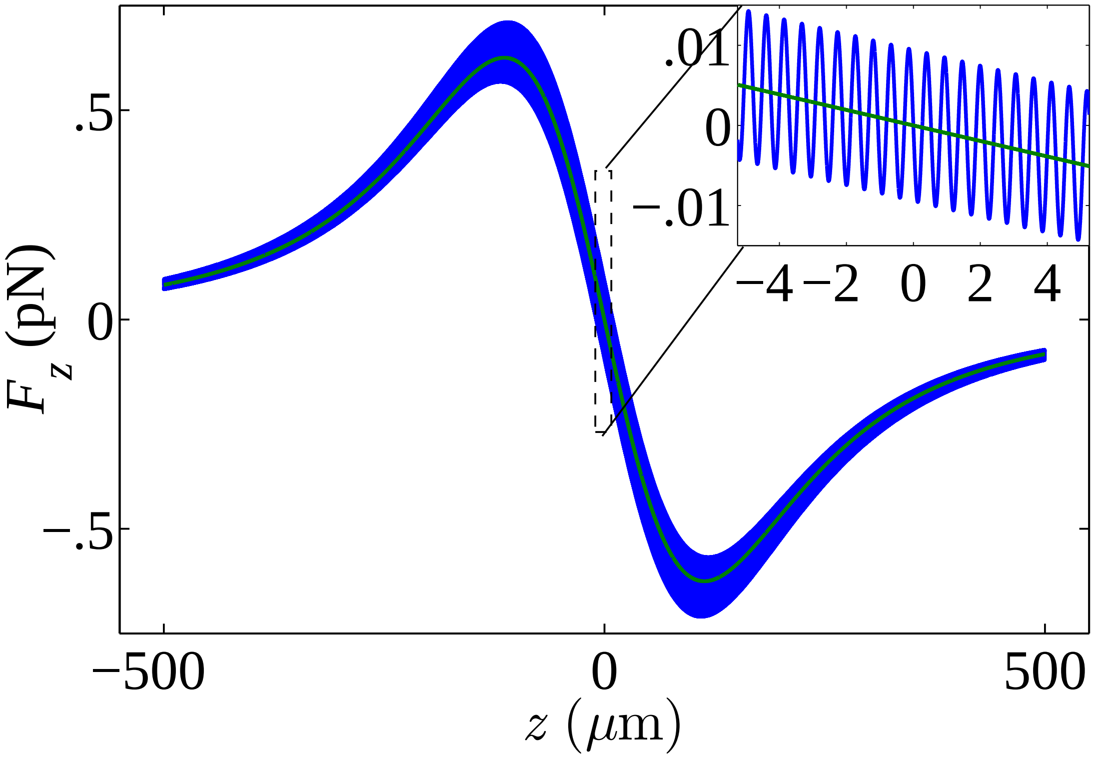

Figure 2.3: Using the same parameters as figure 2.2, this simulation looks at only the force applied to the nano-sphere in the center of the beam profile i.e. when $x, y = 0$. The x axis zero is the the center of the two foci. In the upper righthand corner is close up of 10 μm span in the center of the two foci. This is shown to illustrate the force modulation resulting from the intesity modulation leading to an optical standing wave. Where the force is zero there exists multiple trapping sites along the beam path. The green line is the force profile the nano-sphere experiences in the absence of light interference; figure from reference[42].

The nano-spheres are loaded into the optical standing wave trap and can be persistently trapped at low vacuum notwithstanding some external perturbation. As seen from figure 2.3, there exist multiple trapping sites in the dual beam optical standing wave. We have seen, experimentally, that multiple nano-spheres can be trapped into two different trapping sites between the foci, and single spheres can even move between optical potential wells. These findings further the support of the large range of possible trapping positions in the ”shallow” optical standing wave trap. Despite the multiple sites, and some uncertainty to the exact site the nano-sphere is loaded into, the optical standing wave does provide some advantages discussed later.

2.2 Nano-sphere Loading

To load the nano-spheres into the dual beam optical standing wave trap, we use a piezo driven glass slide cantilever to create a dry aerosol of nano-spheres off of the glass slide and into the space directly above the center between the two lasers’ foci. To prepare the glass slide we employ two slide preparation methods. In the first method, a transfer slide is made by desiccating a solution from Bangs Laboratories, Inc.[57] of .3 μm fused silia nano-spheres at 150 C for 15 minutes. The nano-spheres can then be transferred to individual slides where they are ”smeared” onto the end of a prepared slide. The second method of preparing the slides requires a solution made of a single drop of the bead solution of 10% solids with .5 ml of deionized water. Two drops of that solution are placed about a centimeter from the edge of the slide. The slide is placed at the end of the vacuum head of a spin coater lined with aluminum foil to prevent silica nano-spheres from contaminating the vacuum attached[58]. The slide is prepared by spinning at 500 rpm for 10 seconds, then at 3000 rpm for 60 seconds[59]. Before loading the prepared slide into the piezo driven mount, the slides are baked again at 150 C for 15 minutes and are loaded ”hot”. Due to the physical space constraints caused by optical cavity in the vacuum chamber, the slide is put in contact with a ring piezo at an angle.

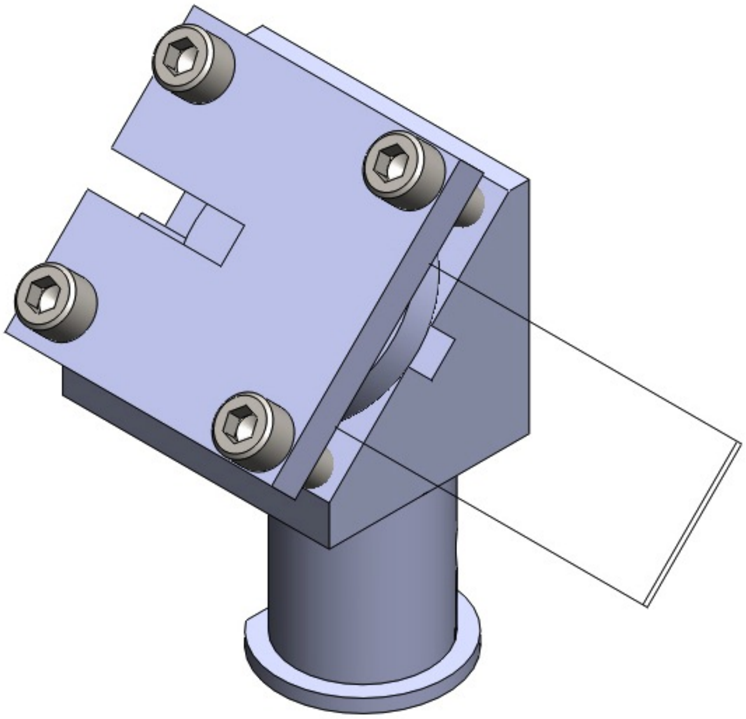

Figure 2.4: A SOLIDWORKS drawing of the piezo glass slide mount to load nano-spheres into the optical standing wave traps. The slide is placed just above the piezo and is clamped down with the Techtron®plate with slots for electrical connection to the piezo ring.

The ring piezo is manufactured by APC International Ltd.[60] with an outer diameter of 38 mm, and an inner diameter of 13 mm, and a width of 6.35 mm. The piezo is clamped down onto an aluminum mount with Techtron®. In order to overcome the stiction forces holding the dry nano-spheres to the glass slide, the piezo is held at 30-90 V and then oscillated at approximately 142000 Hz or 339000 Hz corresponding to two resonant modes of the piezo[61]. A Solidworks rendering of the piezo ring and slide mount is shown in figure 2.4.

2.3 Imaging

In order to deduce the force experienced by the nano-sphere, we need to image its motion. To accomplish this task we employ a technique that tracks the motion of the laser light scattered by the nano-sphere. Ideally we would like to see the motion of the nano-sphere in all three dimensions and it is for this reason the scattered light is collected by two high numerical aperture lenses placed near the trap site. The vertical imaging axis has a 25 mm focal length lens[62] placed in a custom vacuum compatible lens tube, designed and machined in house. The lens tube is mounted in a ∼25° angled v-block that is oriented toward a vacuum chamber window. The second imaging lens is inside a custom lens tube in the optical breadboard directly below the nano-spheres trap site. This lens images the nano-sphere's motion along the standing wave axis in what we call the axial or z axis, and radially out from the beam path in what we call the horizontal axis or the x axis. As the nano-sphere moves in those two axes, the motion is recorded in the scattered light collected and collimated from the lens below, and is then projected to a quadrant photodetector. The quadrant photodetector is a large area circular InGaAs photovoltaic, separated into four quadrants as seen in figure 2.5[63].

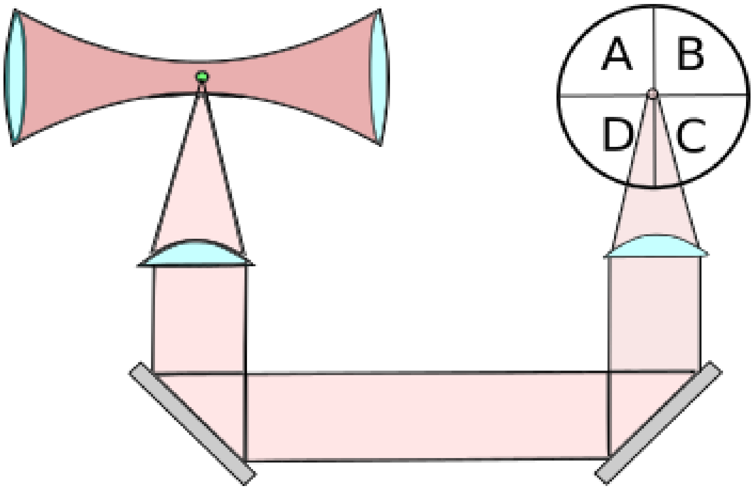

Figure 2.5: In order to deduce the center-of-mass motion of the nano-sphere, scattered light is collected over a solid angle, via two lenses of numerical aperture 0.25, and then focused on to two quadrant photodetectors (QPDs) to record the three dimensional motion. Here is a graphical representation of the first stage of the data collection of the center-of-mass motion of the nano-sphere.

Each quadrant photodetector is connected to a quad operational amplifier[64] acting as a transimpedence amplifier inside the head of the photodetector. The four quadrant voltages are then sent to a single custom built-in-house box that will compute a sum of all four quadrant signals, a combination of sums and differences using 6 operational amplifiers as summing amplifiers and two operational amplifiers used as inverting amplifiers. One difference channel calculates the signals from A + B minus the signals of C + D, which will help with the projected motion along the vertical axis of the photodetector. The other difference channel computes the difference of signals B + C and signals A + D, which will give the projected motion along the horizontal axis of the photodetector[65].

By turning the quadrant photodetector while observing the voltage spectrum, we can minimize cross talk in the signals in each lab axis. This helps us effectively look at the motion of a nano-sphere in a single lab axis on each difference calculation of the quadrant photodetector's signals. If the beam is perfectly Gaussian then the frequencies of the "horizontal" and "vertical" are very similar but not the same due to the polarization dependence on the resonance of the radial traps, one can read more about this dependence in reference[12]. Along the beam axis the frequencies are much higher since the intensity gradient along the optical standing wave is much larger than the radial gradient. Another method of matching the quadrant axes to the lab axes, is to use a crosshair after the high numerical aperture lens and then turn the quadrant axes to match the projected crosshair.

2.4 Force Calibration

In order to deduce the force applied to the levitated nano-sphere we need some way of calibrating the signal voltage to the physical displacement of the nano-sphere. We start by recording 100 s of the nano-spheres motion at a low vacuum. The pressure of the system must be high enough that the nano-sphere's center-of-mass motion is in thermal equilibrium with the surrounding gas. At higher pressures, collisions with air molecules dominate the heating of the center-of-mass temperature of the nano-sphere. Therefore, we can assume the center-of-mass motion of the nano-sphere is at room temperature of $\sim$300 K. After recording the displacement of the nano-sphere over 100 s, we perform a fast Fourier transform (fft), which gives us both a real and imaginary parts of the measurement. In conjunction, the real and imaginary parts give us both the magnitude and the phase of the displacement, which we take with respect to a reference signal. We can now construct the voltage spectral density using the real and imaginary parts of the measurement. Checking the voltage spectrum at multiple pressures, we experimentally found at a pressure above 2 Torr that the nano-sphere is in fact in thermal equilibrium with the surrounding gas.

Then using the "thermal" voltage spectrum shown in figure 2.6, we can calibrate a displacement to quadrant voltage ratio, with the assumption of a linear relationship between voltage on the quadrant photodetector and the nano-sphere's motion. To ensure that we are well into the equilibrium temperature with the surrounding gas, and in a regime where the cooling is dominated by collisions, we choose a pressure of 6 Torr as our thermal file. We can use the equilibrium temperature to solve for the quality factor using a Lorentzian fit on the "thermal" voltage spectrum.

The functional form of the Lorentzian fit for the position spectral density dependent on frequency f is:

$$S^{1/2}(f) = \sqrt{\frac{4k_bT}{Qm}\frac{1}{({\omega_0}^2-(2\pi f)^2)^2+(2\pi f)^2/Q^2}}\,[66] \tag{2.5}$$

where k_b is the Boltzmann constant, T is the temperature, Q is the quality factor, m is the nano-sphere mass, and ω_0 is the resonant frequency. Using room temperature we can ascertain the quality factor Q and the frequency $f_0 = \omega_0/2\pi$ from the Lorenztian fit. Then we are able to deduce the thermal distance the nano-sphere travels by using the thermal motion of a nano-sphere in an optical trap expressed as:

$$x = \sqrt{\frac{4\,k_b\,T\,Q\,b}{m(2\,\pi\,f)^3}} \tag{2.6}$$

Using the thermal motion x divided by the voltage signal, we calculate a ratio of m/V. Experimentally the value of the displacement and voltage ratio ranged from

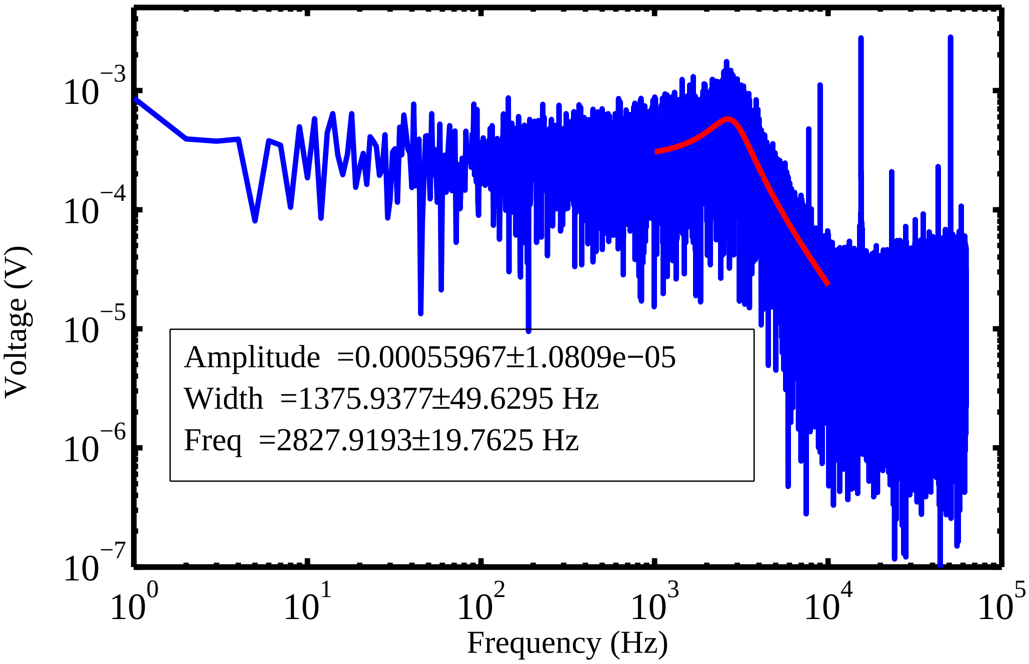

Figure 2.6: This is the "thermal" voltage spectrum of a 300 nm diameter nano-sphere trapped in the optical standing wave trap at 6 Torr. At this pressure the temperature of the center-of-mass motion of the nano-sphere is in equilibrium with the room environment. The red line is the Lorenztian fit used to calculate the quality factor of the optical standing wave trap to help us ascertain the nano-sphere displacement to voltage ratio.

10^{-6} to 10^{-5} m/V We now know the ratio between the nano-sphere's motion and the voltage signals from the quadrant photodetectors. Using this ratio and the voltage spectrum we can find a position spectrum of the nano-sphere. From the nano-sphere's motion we can then deduce the force experienced by the nano-sphere. This is done by tracking the motion of the sphere and using the restoring force felt by the nano-sphere from the optical standing wave trap. Using Hooke's law, $\mathbf{F} = k\,\mathbf{x}$, where the spring constant of our optical trap is $k = m\,\omega_0^2$, m is the mass of the nano-sphere, and ω_0 is the angular frequency, we can define the force applied to the nano-sphere.

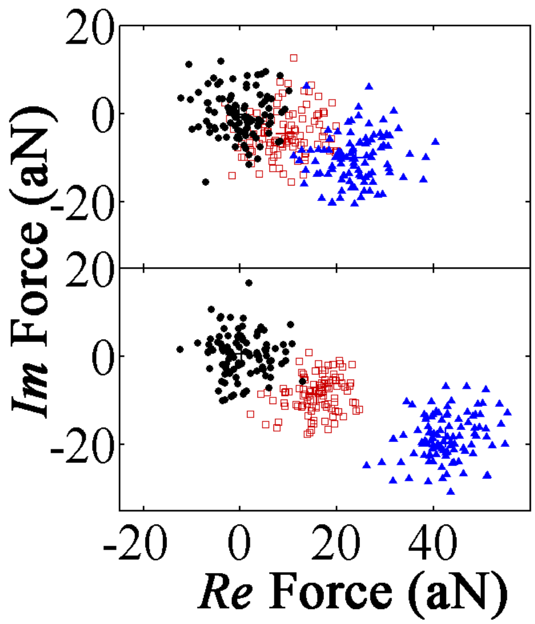

Figure 2.7: Scatter plots of the real and imaginary force measured for two 300 nm diameter nano-spheres. The nano-spheres were charged with a single electron (top) or two electrons (bottom) on their surface. Using the signal of the driven electric field as a reference, the real and imaginary force measurements give the magnitude and the phase of the measured force. The nano-spheres where subject to 0 V, 12 V, and 28 V driving on two tungsten electrode placed 1 cm from a planar gold mirror. The nano-spheres are trapped approximately 2 mm from the gold mirror.

As nano-spheres are loaded in the trap, 10% of those have some residual charge on them. To calibrate the motion of the signal, we can use a driven electric field to drive the motion of the charged nano-sphere. The resolution of the imaging system can differentiate between singly or multiply charged nano-spheres. In figure 2.7 one can see the scatter plot of 100 measurements of the real and imaginary force measurements for two separate spheres driven at two electric fields in red and blue and no electric field in black. The top is a singly charged nano-sphere while the lower is a doubly charged nano-sphere. The phase of the two nano-spheres is similar which in this case means that the two sphere's charge had the same sign. The singly charged nano-sphere had a displacement to voltage ratio of $\sim 2\times10^{-6}$ m/V where the doubly charged sphere's ratio was $\sim 1.4\times10^{-6}$ m/V. The nano-spheres were driven at a pressure of 2 Torr by applying 0 V, 12 V, and 28 V to tungsten rods 1 cm away corresponding to electric fields of 0 V/m, 1000 V/m, and 2300 V/m respectively. If we look at the Coulomb force on the spheres the force and electric fields correspond to approximately 1 and 2 electrons on the spheres.

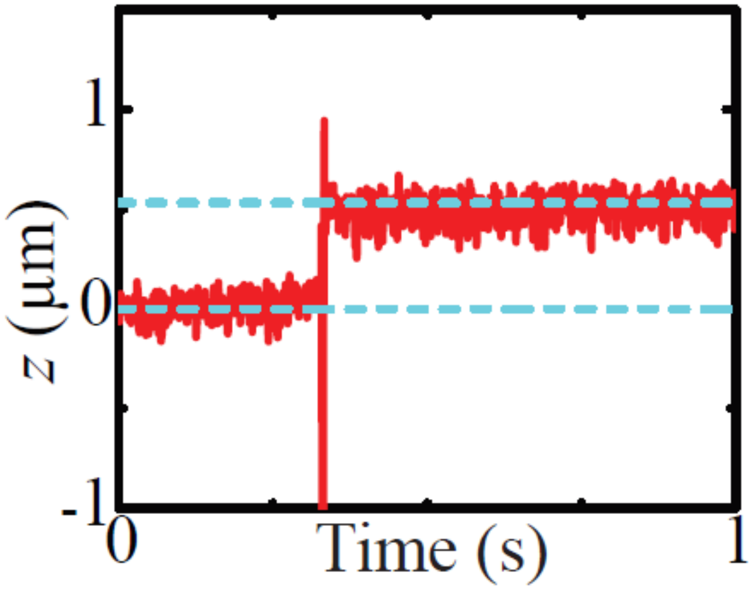

Figure 2.8: Time signal of the nano-sphere "jumping" from one trapping site in the optical standing wave to the adjacent site. Here the trapping laser provides the distance to voltage calibration since the site spacing is defined by $\lambda/2$. This is a possible calibration method that is independent of the charge present on the nano-sphere[42].

Beyond that calibration we have been able to perturb the nano-sphere with radiation pressure to adjacent trapping sites in the optical standing wave trap. We use the feedback cooling laser at 780 nm to "kick" the nano-sphere to the next site. The advantage of this method is that it works with the trapped nano-spheres that are neutral. In figure 2.8 the resonant frequency of the trap was 4258 Hz with a Q of $\sim$2, and a displacement to voltage ratio of 1.52×10^{-6} m/V. These experimental parameters give the displacement of 514 nm ± 43 nm.

2.5 Cooling and Reaching High Vacuum

As stated in the introduction, the sensitivity of our force measurement has dependence on the temperature and the quality factor. One way we plan to increase our force sensitivity is to cool the center-of-mass motion of the bead and in tandem reduce the thermalization of the nano-sphere with the surrounding environment through evacuation.

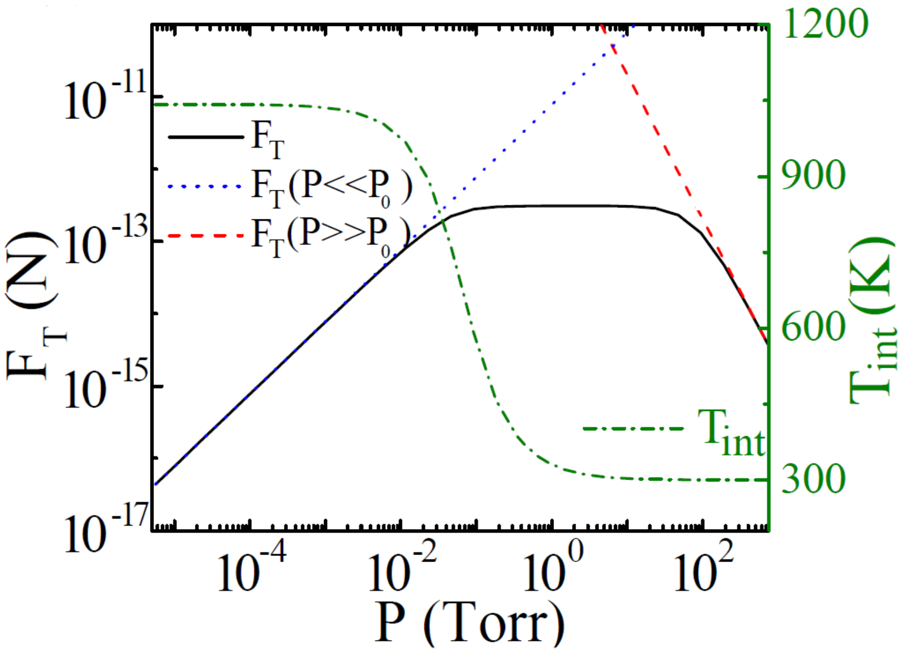

Figure 2.9: The photothermal force F_T is plotted vs pressure, this model is adapted from Fuchs[67]. The dotted blue line represents the photothermal force in the diffusive regime where the micro-sphere is cooled through blackbody radiation. The red line represents the ballistic regime where cooling is dominated by the collisions with the surrounding gas molecules. The temperature in green accounts for optical absorption of the bulk silica assumming a complex permittivity $\epsilon = \epsilon_1 + i\epsilon_2$ where ϵ_2 parameterizes the optical absorption of silica. For these models we assume $\epsilon_2 = 10^{-6}$ and a 1% internal temperature gradient across the sphere. $P_0 = \frac{3\eta}{r}\sqrt{\frac{R_{gas}T_{gas}}{M}}$ which is the pressure at which the pressure transitions from a diffussive regime to a ballistic regime[43].

If you look at the model of the internal temperature of the nano-spheres in figure 2.9 the temperature increases around a pressure of 1 Torr. This model assumes that the intensity of the 1064 nm trapping laser is 2×10^9 W/m^2, and $\epsilon_2 = 10^{-6}$, where ϵ_2 parameterizes the optical absorption of silica and is the imaginary part of fused silica's permittivity. Depending on the value of ϵ_2, the temperature graph shifts left or right depending on its pressure dependence, but the overall shape stays the same.

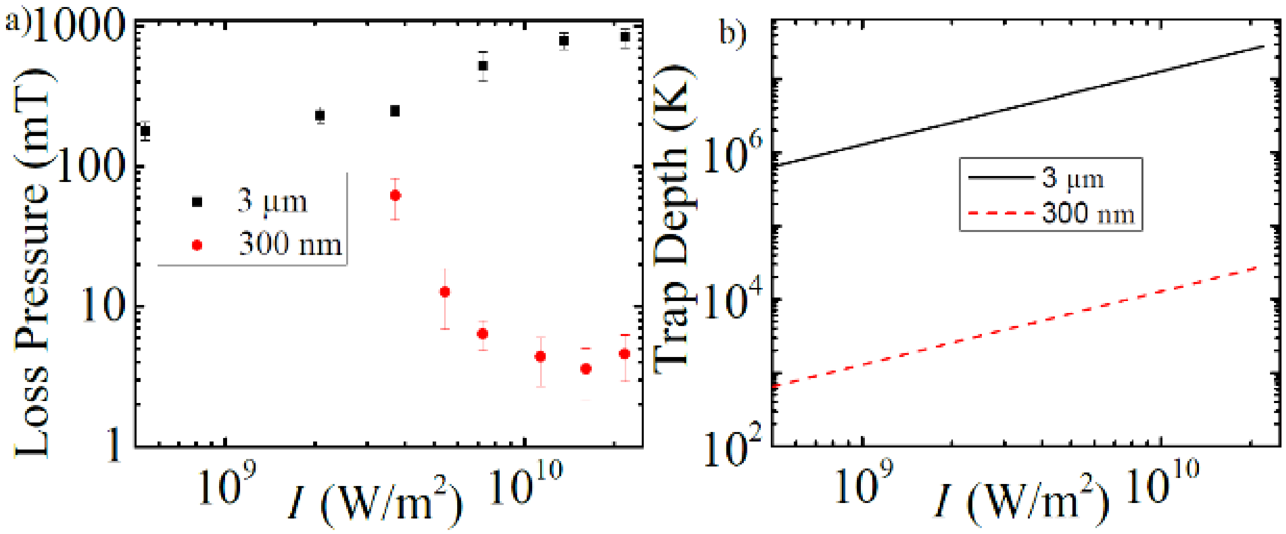

Figure 2.10: (a)Mean pressure at which beads are lost from the trap for various laser trapping intensities with no laser feedback-cooling applied. Statistics are shown for 30 beads of each size. (b) Calculated trapping depth for 300 nm and 3μm beads[42].

If no attempt of cooling the center-of-mass motion of the nano-sphere is made, the transition from a diffusive pressure regime to a ballistic regime, the nano-sphere is lost from the trap. This occurs because the damping from the surround gas on the motion of the nano-sphere becomes smaller as the radiometric forces remain the same, causing enough heating of the center-of-mass motion to overcome the trap depth. In figure 2.10a the mean pressure at which that loss occurs at different laser intensities is shown. As indicated in reference[43], we believed the main cause for bead loss for the 3 μm diameter nano-spheres is due to radiometric forces. The temperature gradients across the nano-sphere cause enough of a perturbative flow of the surrounding gas that the bead is forced from the optical trap. As the intensity of the laser increases, this effect is increased. However, the case for the 300 nm diameter nano-spheres is the higher the intensity, the lower pressures that can be reached in the absence of the feedback-cooling. We believe that radiometric forces are still the cause for the nano-sphere being lost. Due to the smaller size of the spheres, the temperature gradients are smaller and thus the radiometric forces are weaker. However the smaller nano-spheres have the sharp increase in loss pressure at intensities around 4×10^9 W/m^2, this is most likely due to the reduced trap depth of the 300 nm spheres. Once we reach higher vacuum the applied feedback cooling can be lowered by reducing the power of the feedback lasers. This indicates that similar to the case of the 3 μm micro-spheres radiometric forces are the cause of the nano-sphere loss. As for the 300 nm spheres they are lost at higher vacuum in the absence of feedback cooling, we believe this has to do with the reduced trap depth for the smaller nano-spheres as indicated in figure 2.10b[42].

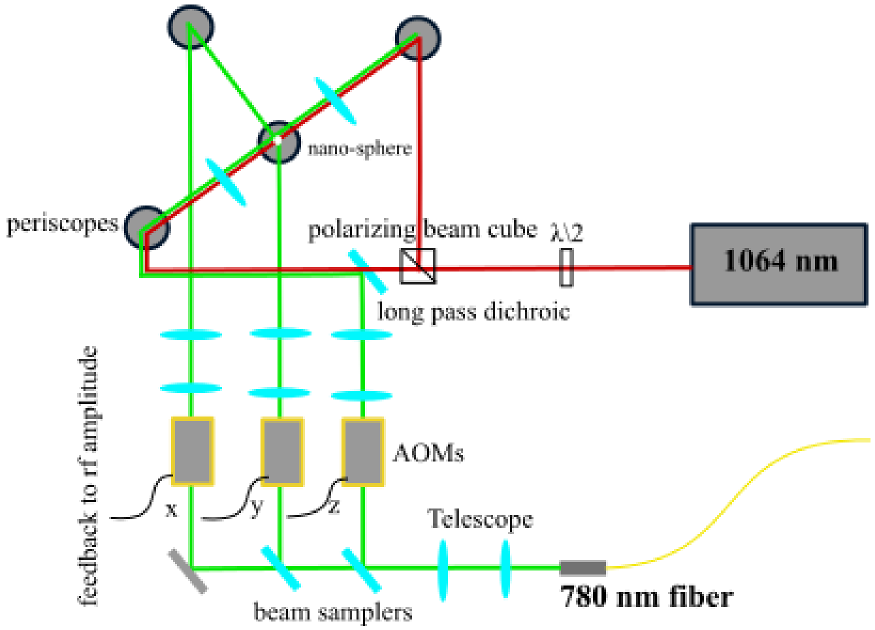

Figure 2.11: The 1064 optical standing wave trap in red is combined with a portion of 780 nm light along the trap axis cooling the ’z’ axis. Some of the power is reflected up a periscope from underneath the nano-sphere to cool the ’y’ axis. And the remainder of the power is delivered orthogonal to the other axes in the ’x’ direction. Each laser is focused down by lenses to the bead, the ’x’ and ’y’ focusing lenses are not shown. The bead’s motion is recorded and phase shifted to get an instantaneous velocity signal. That signal is used to modulate the rf amplitude of the acousto optic modulators, cooling their respective axes.

To cool the motion of the nano-spheres in our system, we employ three dimensional active feedback cooling. This cooling scheme uses three separate 780 nm lasers modulated with acousto optic modulators (AOM). The optical path of the active feedback is illustrated in figure 2.11. The cooling method works with the feedback by phase shifting the displacement signal to a velocity signal, which is then used as a feedback signal to the 780 nm laser to effectively change the center of the optical trap. As the nano-sphere's velocity points away from the trap, the trap center will move to compensate for the beads velocity and apply a velocity dependent force in the opposite direction of the nano-sphere's velocity. Thus cooling the center-of-mass motion of the nano-sphere. The minimal detectable force is shown in section 2.6.2, is inversely proportional to the quality factor Q, and proportional to the temperature T. The feedback cooling process effects both the temperature and the quality factor of the optical standing wave trap. Since the effects of the feedback cooling are equivalent in both cases, there is no loss or gain in the minimal detectable force.

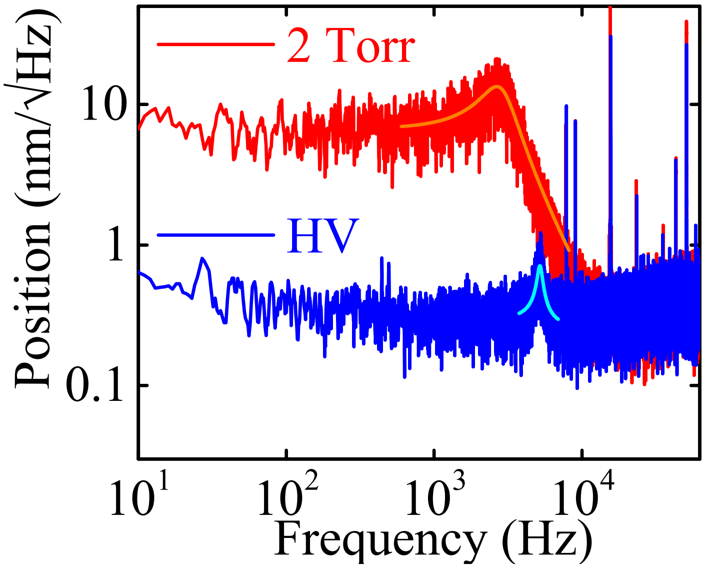

Figure 2.12: Two position spectra of the same 300 nm diameter nano-sphere before and after cooling and transitioning from low vacuum (2 Torr) to high vacuum (HV) (5×10^{-6}Torr). The Lorentzian fits show cooling from ~300 K at 2 Torr to 460 mK at HV; figure adapted from reference[42].

Once the center-of-mass motion is cooled, we acheive high vacuum by using a turbomolecular pump to start slowly taking the air out of the chamber through a cracked large valve. The air is pumped out till we reach a pressure of approximately 500 mTorr. At that point, we open a large valve even more to evacuate the chamber faster with the turbomolecular pump. Once the pressure is $\sim 10^{-5}$ mbar we reduce the feedback cooling applied to the nano-sphere and reduce the total laser power in the trapping beams from 1.3 W to 1.1 W. Finally, the valve can be opened all the way to speed up the pumping process reaching a final pressure on the order of 10^{-6} Torr. One can observe the effect of evacuation and applied feedback cooling in figure 2.12[42].

2.6 Results

2.6.1 Trap Stability at High Vacuum and Measurement of Bead Heating Rate

Once the bead is at high vacuum, the heating due to radiometric forces are reduced dramatically and the nano-sphere can be held in the optical standing wave trap with little feedback cooling applied. The power of the optical trap can be reduced. With lower intensities around 10^{10}W/m^2 the trap is stable indefinitely, we have shown averaging times of 10^5 s, but as the intensity of the trap is increased the lifetime of the trap decreases as shown in figure 2.13a. The linear fit in green shows an exponential reduction in lifetimes. Figure 2.13b shows that even for a range of $\epsilon_2 = (2.5 \times 10^{-7}, 1 \times 10^{-6})$ the internal thermalization is short, under 0.1 s ruling out evaporation or loss due to laser heating[42].

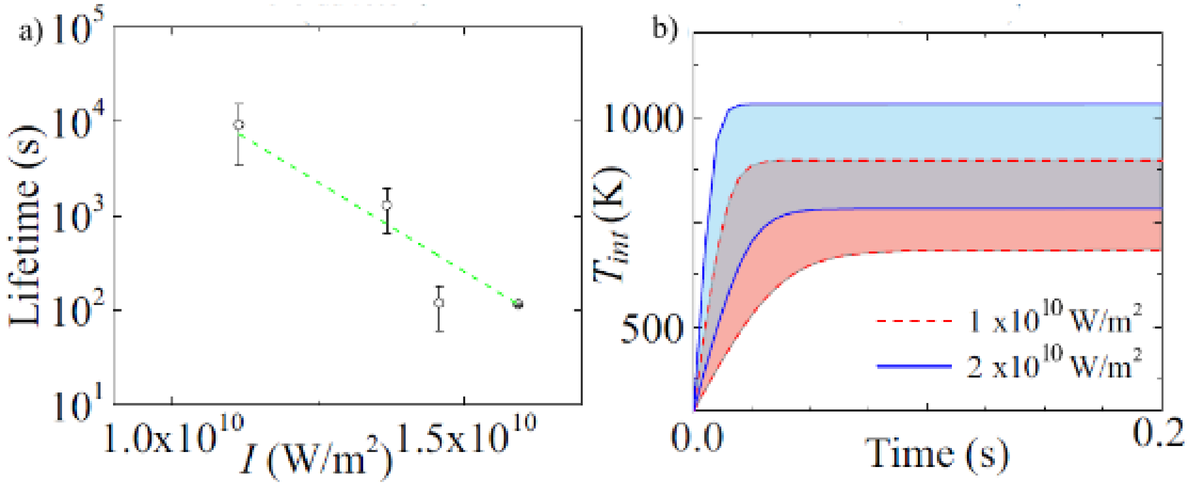

Figure 2.13: a)Lifetime vs Laser Intensity for nano-spheres at high vacuum with a linear fit in green. b)Expected internal temperature rise for a 300 nm nano-spheres for two intensities. The bands account for a range of $\epsilon_2 = (2.5 \times 10^{-7}, 1 \times 10^{-6})$[42].

The exact loss mechanism is uncertain, but one hypothesis is the nano-sphere undergoes an annealing over time phase change, which could bring a kick due to a sudden change in size, density, or refractive index[42]. This hypothesis is based on the reports of silica annealing at lower temperature over similar time scales of the trap lifetimes we observed[68].

Again, at high vacuum with lower laser power, we have shown optical standing wave trap lifetimes over several days with feedback cooling applied to the nano-sphere. In figure 2.14 we actually are able to look at the nano-spheres motion at high vacuum after we cease applying feedback. This allows us to ascertain the heating rate of the center-of-mass motion of the nano-sphere.

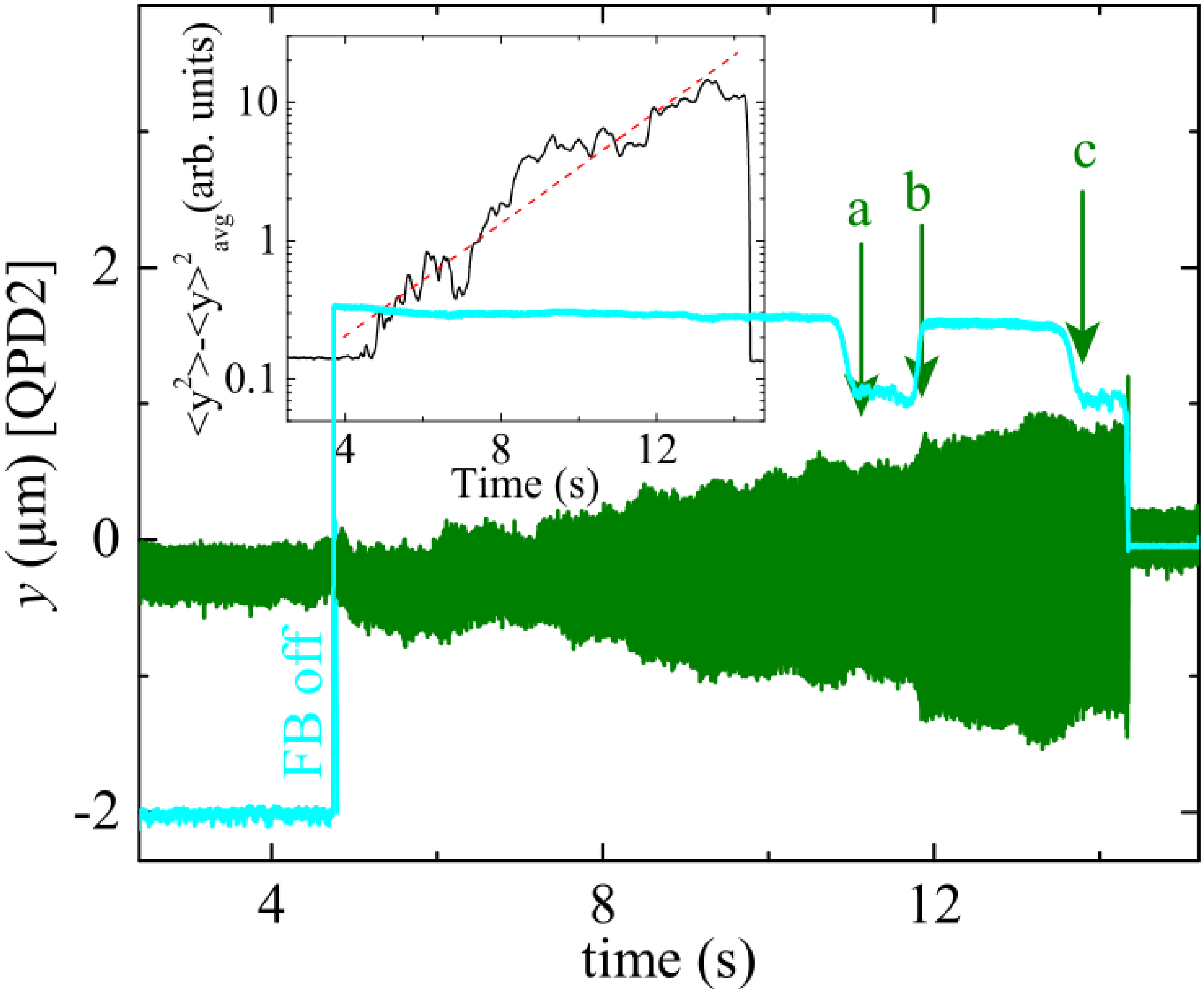

Figure 2.14: The green is the measured motion of a nano-sphere in the 'y' axis or the vertical axis. The blue is the motion of the nano-sphere in the 'z' axis along the trapping beam propagation. Due to the heating, the blue trace shows that at points a, b, and c the nano-sphere hops between adjacent trapping sites before it is lost. The upper left has the envelope of the averaged variance with an exponential fit[42].

If you look at figure 2.14 you can see at points a, b, and c the nano-sphere hops to adjacent trapping sites due to the heating before it is lost. In the upper left hand corner there is an exponential fit of the envelope of the average variance showing a heating rate ~ 0.4 s^{-1}. This is the observed rate for the oscillator's energy e folding time. In the absence of laser noise and the non-conservative scattering heating, the rate from gas collisions to reach the thermal bath energy is approximately 1×10^{-2}s^{-1}, assuming the nano-sphere has a density of 2200 kg/m and a radius of 150 nm; and the surrounding gas is at a pressure of 5 $\times 10^{-6}$ torr with a mean speed of 476 m/s. The heating due to photon recoil is 2 orders of magnitude slower than the rate from gas collisions, which leads us to believe that the heating mechanisms are laser noise and nonconservative scattering forces[42][69].

2.6.2 Zeptonewton Force Measurement

Performing the force measurement in the horizontal direction at high vacuum allows us to take advantage of the reduced damping in the surrounding gas. The minimum detectable force for a harmonic oscillator in equilibrium with a thermal reservoir is

$$F_{min} = S_F^{1/2} b^{1/2} = \sqrt{\frac{4k_b T b k}{\omega_0 Q}} \tag{2.7}$$

where $S_F^{1/2}$ is the thermal noise force spectral density, k_b is the Boltzmann constant, T is the temperature of the center-of-mass motion of the nano-sphere, b is the measurement bandwidth, k is the spring constant, ω_0 is the angular frequency and Q is the quality factor of the oscillator.

To measure the force we used the method described in the force calibration section. The figure 2.15 shows the force measured over time for 3 nano-spheres. The red diamonds show a nano-sphere with two electrons attached, where the blue symbols correspond to a nano-sphere with a single electron, and the black square is an uncharged electron with an averaging time of 10^5 s at high vacuum. We measured the thermal noise force spectral density, $S_F^{1/2}$, is 1.63 ± 0.37aN/Hz$^{1/2}$. With the long averaging time reducing the force sensing level, we were ultimately able to achieve a measured force sensitivity of 5.8 ± 1.3zN.

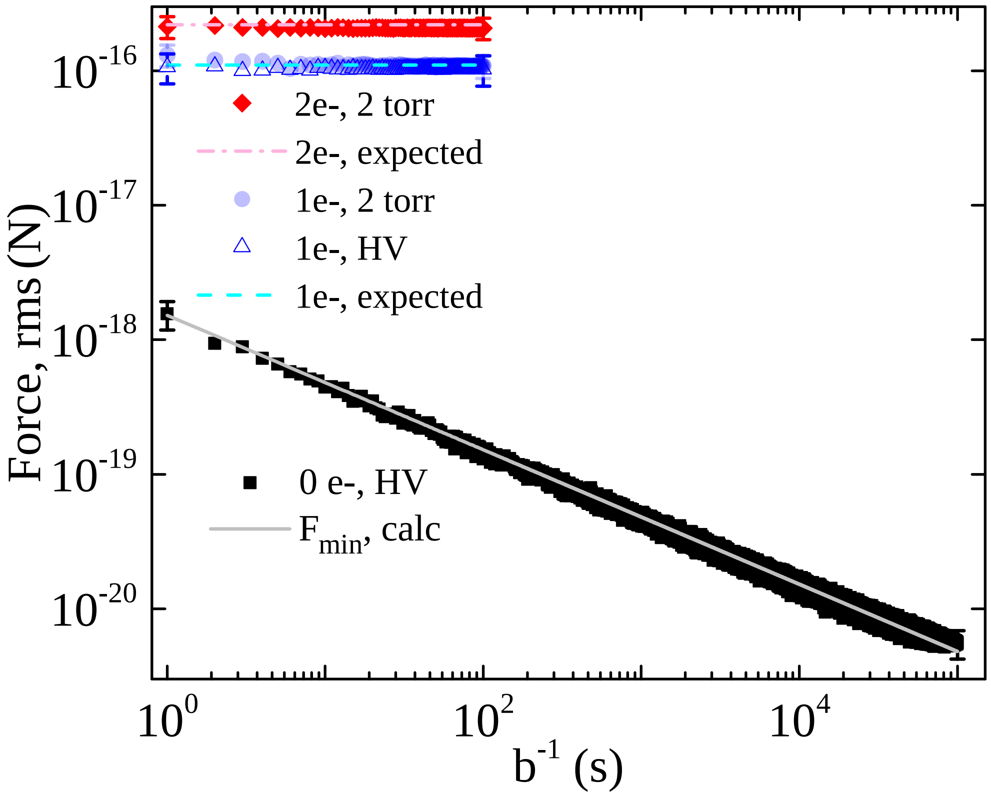

Figure 2.15: Measured force on neutral, singly, and doubly charged nano-spheres with a sinusoidally driven electric field of 1 kV/m. HV corresponds to a vacuum pressure of 10^{-6} mbar. The expected force measurement for the charged spheres is based on the driven electric fields applied Coulomb force. The calculated F_{min} is the experimental parameters as input in Eq. 2.7

For the charged spheres, the force levels out at the Coulomb force $F = q \times E$ where q is the total charge and E is the driven electric field. The singly charged nano-sphere was measured at both 2 Torr and high vacuum. The expected force for the charged nano-spheres falls in the error of the measurement as seen by the dotted lines in figure 2.15.

Chapter 3

Cavity Optomechanics

3.1 Cavity System

The experimental cavity is a hemispherical cavity with a finesse of ∼190. This cavity is housed in an aluminum block with access for the dipole beam path that crosses the cavity axis in the transverse direction. There is also access above for loading the nano-spheres into the optical standing wave traps and below for imaging the nano-sphere's motion. The optical trapping beam is aligned to the cavities fundamental mode. The length of the cavity is locked with the coupled mode to keep the beam's coupling to the cavity and length of the cavity constant. The initial cavity mirror controls the cavity length through a feedback system and a ring piezo on the mirror. In figure 3.3 a high voltage ramp is applied to the ring piezo to span 3.2 μm which is two free spectral ranges (FSRs) of the trapping beam in black and three FSRs of the cooling beam in red. The trapping beam coupled such that approximately 25 percent of the total power of 250 mW incident on the cavity is missing in the reflection signal. The cooling beam has similar coupling with an incident power of 25 mW.

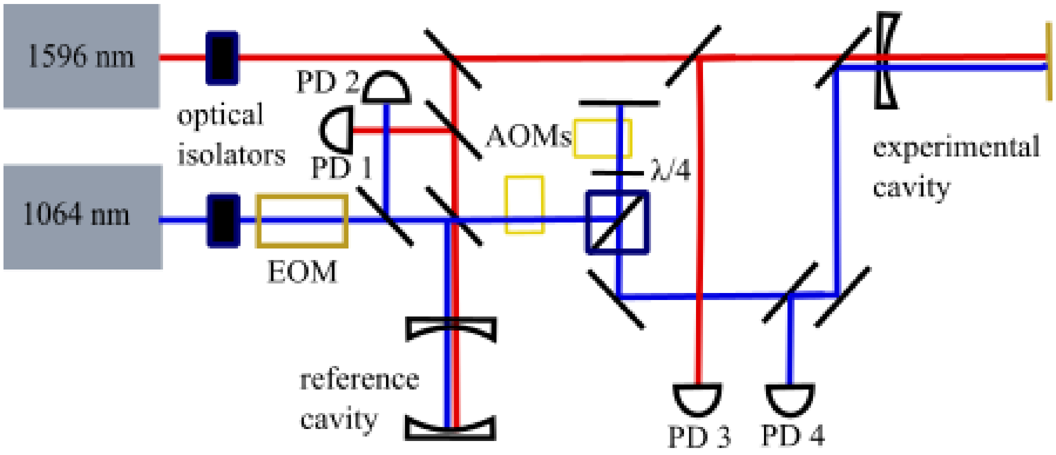

Figure 3.1: Overview of stabilization system. The 1064 nm beam is modulated using the electro-optic-modulator (EOM) in the beam path at 10 MHz, Photodetector (PD 2) is the reflection readout from the reference cavity used in locking the frequency of the laser. Similarly, photodector (PD 1) has the reflection signal from the reference cavity associated with the 1596 nm beam. In the 1064 nm path there is a single pass of the acoustic optical modulator (AOM), and a double pass AOM to achieve a frequency shift of the 1064 nm beam to ensure sideband cooling of the nano-sphere in the experimental cavity. Photodetector 3 (PD 3) has the drift information of the length of the experimental cavity and is used to stabilize the length of the cavity. The cavity readout as seen in photodetector 4 (PD 4) has information of the motion of the nano-sphere as its' motion modulates the cavities length.

3.2 Cavity Coupling

One observes in figure 3.1 that our system includes two cavities, a reference cavity that is used as a length reference for the wavelength of the 1064 nm[70] and 1596 nm[71] lasers that are incident on the other experimental cavity. In one case we have a concave-concave geometry cavity and a hemispherical cavity. In order to couple the laser light to the TEM_{00} mode, or fundamental mode of the cavity, we must align the beam to the center of of the cavity and ensure that the beam is antiparallel with its reflection. We must also ensure that the laser is mode matched to the cavity. Mode matching to an optical cavity is that the incident laser's beam waist (w_0) and the cavity waist match in size and position. The cavity waist is defined as the point at which the laser wave front should be planar. Another way of thinking about mode matching is literally matching the lasers wave fronts to the curvature of the cavity mirrors.

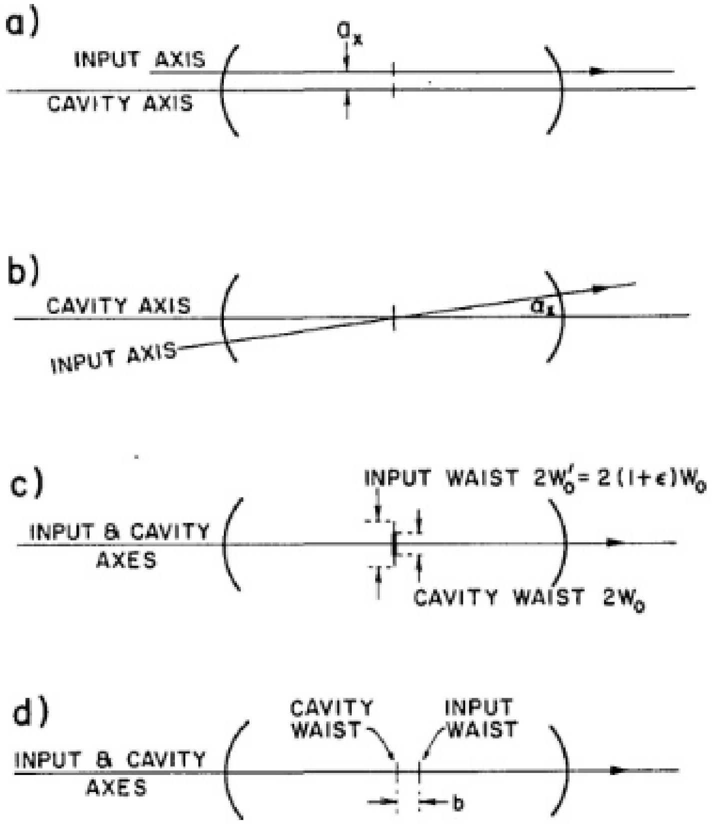

Figure 3.2: Example of cavity misalignment. In the cases of a) and b) the misalignment is due to steering into the cavity. For the cases c and d the misalignment is an issue with mode matching with the cavity; figure from reference[72]

In the case of our reference cavity, we have a concave-concave geometry cavity implying that the cavity waist is in the center of the two cavity mirrors. In the case or our experimental cavity, it is a hemispherical cavity and the cavity waist is on the surface of the planar mirror. In both cases, the waist size is defined by the cavities mirror's geometry i.e. the distance between and the curvature of the cavity mirrors, and the laser wavelength (λ). Using the equation for the radius of curvature:

$$R_c(z) = z\Big[1 + \Big(\pi \frac{w_0^2}{\lambda z}\Big)\Big] \text{ [73]} \tag{3.1}$$

We know the radius of curvature from the cavity mirrors and z is the distance from the cavity mirror to the cavity focal point or waist. In the case of our concave-

concave geometry reference cavity the two mirrors have the same focal length and therefore the same radius of curvature making the cavity waist in the center of the two mirrors. As previously mentioned, the size of the beam at the mirror surface is also defined by the cavity geometry and laser wavelength. This is the because the waist depends on the Rayleigh range $z_r = \frac{\pi w_0^2}{\lambda}$ which means it ultimately depends on the cavity/beam waist. The equation below defines the diameter of the beam dependent on: the beam waist w_0, the distance to the cavity mirrors from the waist z, and the laser wavelength λ.

$$w(z) = \sqrt{w_0^2\left[1 + \left(\frac{z}{z_r}\right)^2\right]} = \sqrt{w_0^2\left[1 + \left(\frac{\lambda z}{\pi w_0^2}\right)^2\right]} \text{ [73]} \tag{3.2}$$

We use a collimated beam with a beam diameter that matches the beam $1/e^2$ radius we calculated from $w(z)$. We use the beams angular width definitions and the small angle approximation to find:

$$\tan\theta \approx \theta = \frac{D}{F} = \frac{4\lambda}{2\pi w_0} \Rightarrow D = \frac{4F\lambda}{2\pi w_0} \tag{3.3}$$

where D is the diameter of the beam of wavelength λ on the lens of focal length F. With those parameters defined you can begin aligning the cavity by walking two mirrors and adjusting a mode matching lens. In the case of the reference cavity the R_c of the cavity mirrors was 50 mm and the cavity length was slightly less than 10 mm. We decided to use a 300 mm focal length lens, with an anti-reflection coating for both 1064 and 1596 nm, on a linear mini translation stage to adjust for mode matching, the diameter of the 1064 nm beam on the 200 mm lens is 3 mm where the 1596 is 4 mm corresponding to the cavity waist of 130 μm and 150 μm respectively The experimental cavity is ~4.98 cm in length and the mirrors R_1 is 50 mm on the near infrared (NIR) coated mirror and a planar gold mirror with $R_c = \infty$. The mode matching lens we choose has a focal length of 300 mm to fit in the crowded optical layout. The radius on that mode matching lens for the experimental hemispherical cavity is 8 mm for the 1596 nm and 6 mm for the 1064 nm. The cavity waist is 40 μm and 30 μm respectively.

As one begins to align the optical cavity, there are multiple configurations that lead to coupling of higher TEM modes. Once you minimize the misalignments shown in figure 3.2 you will start to see coupling in the lower order modes separated by a free spectral range of the cavity. The reference cavity has a free spectral range of 15 GHz where the experimental cavity has a free spectral range of 3 GHz. In order to align the cavity to the fundamental mode, we need to know the mode currently being aligned and optimized. Our optical cavities are non-degenerate and the modes of the cavity are separated in frequency by:

$$\nu_0 = \frac{c}{2d}\frac{1}{\pi}\arccos\left(\left(\left(1-\frac{d}{R_1}\right)\left(1-\frac{d}{R_2}\right)\right)^{1/2}\right) [72] \tag{3.4}$$

The frequency separation of the reference cavity, ν_0^{ref}, is 1.4 GHz. The alignment procedure of the reference cavity is assisted with the addition of a CCD camera. The camera is set up to show the transmission of the concave-concave geometry cavity. By checking the mode structure of the transmitted laser, you can see if you are moving to a higher mode or a lower mode. In the case of the experimental cavity one must look at the structure or the reflection signal while the piezo is expanded by more than one free spectral range. As the lower order modes of the cavity are aligned the coupling becomes more prominent. The separation between modes in the experimental cavity, ν_0^{exp}, is also 1.4 GHz. In figure 3.3 one can see the higher order modes, shown by the smaller peaks, in the red trace of the 1064 nm laser. While aligning the cavity to higher order modes, the next lower order mode becomes apparent at a 1.4 GHz separation from the current optimized mode. Eventually the structure of the ramp scan shows no peak at 1.4 GHz. At this point you have coupled to the fundamental mode of the cavity.

3.3 Laser Stabilization

As previously noted the reference cavity serves as the constant length reference to stabilize the frequency of the two laser systems. Because of the ratio of the two

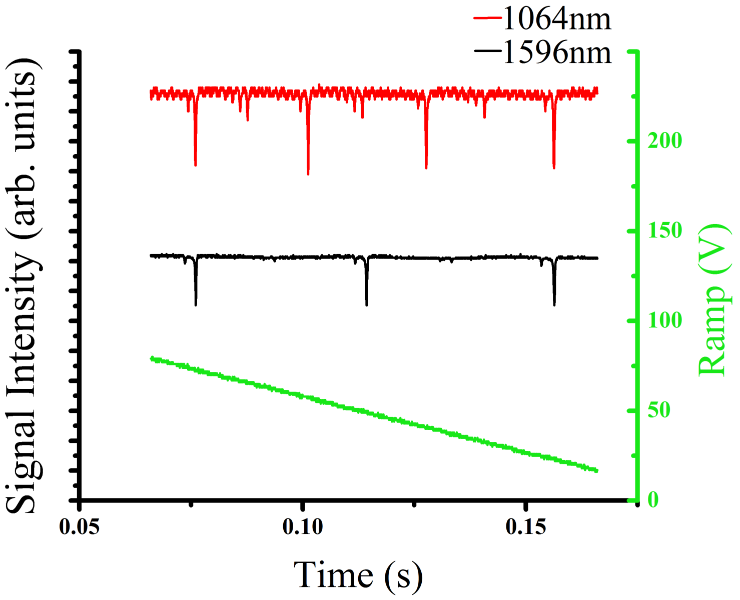

Figure 3.3: A 50 V voltage ramp on the piezo ring of the experimental cavity shown in green. The physical distance corresponds to approximately one wavelength of the trapping laser or 1596 nm. The black is the reflected signal of the trapping laser (1596 nm) where the red is the reflected signal of the cooling/imaging laser (1064 nm).

beams every other fundamental mode of the trapping beam is resonant with a resonant fundamental mode of the cooling beam. The reference cavity is a 10 mm long concave-concave geometry cavity housed in Ultra Low Expansion (ULE) Glass with a finesse of ∼1000. Each beam is mode matched to the fundamental mode of the cavity. Both beams utilize the the Pound-Drever-Hall method of locking the frequency.[74] With an Electro-Optic-Modulator (EOM) in the cooling laser beam line, we modulate the beam with a dither frequency of 10 MHz, the correction signal is then applied to a piezo attached to the laser crystal keeping the frequency constant. The 1596 nm laser servo adds a 4 MHz dither for current modulation on the semiconductor laser diode, in this case the correction signal is used by the current driver to stabilize the frequency of the diode. The frequency stabilized 1596 nm trapping laser is used for the stabilization of the length of the experimental cavity using the same Pound-Drever-Hall technique. The correction signal is fed to the piezo ring behind the curved mirror of the cavity to keep the length of the cavity fixed.

To get the correction signal to lock the 1064 nm laser, the reflection from the reference cavity is incident on a photodiode. In the case of the 1064 nm laser we use FDS100[75] with a 2.2 KOhm resistor in a transimpedence amplifier. The resonance is around 8 MHz for the photodetector, but there is enough speed to get the 10MHz dither on the reflection signal. The signal from the photodetector is then amplified using a mini-circuits ZFL-500 BNC amplifier. Afterwords the 'out' of the amplifier is sent to the radio frequency, 'RF', input of a ZFMIQ - 10D mini-circuits demodulator. The signal from the signal generator that modulates the EOM is sent to a phase shifer MCL JSPHS-12 and then to the local oscillator, 'LO', input of the demodulator. Then the inphase output, 'I', is sent to a low pass filter. The signal is then fed to a PID built in house, details can be seen in reference[76]. From the PID box the signal goes to a custom built ramp box that allows us to change the gain and offset of the feedback signal. The output of the ramp box goes to the AA Labs A-301 HS high voltage amplifier and the amplified feedback signal is sent through a HV limiting circuit voltage divider that keeps the signal between -50 V and 50 V. The feedback goes back to a piezo that is on the crystal of the Nd:YAG Laser.

To stabilize the frequency of the 1596 nm laser the photodetection consists of a transimpedence amplifier using 2.2 KOhms with a InGaAs photodiode[77]. This signal is feedback to the Laser Servo which frequency locks the laser. The locked 1596 nm laser is the reference for length stabilization of the cavity. The experimental cavitie's reflection signal of the 1596 nm laser is sent to a mini-circuits amplifier ZFL-500LN-BNC+. The amplified signal is then sent to the 'R' input of a mini-circuits mixer ZAD-1+. The 'L' input of the mixer has a phase-shifted 4MHz reference from the laser servo of the 1596 nm laser. The 'I' output goes to a PID controller just like the controller in the 1064 nm laser stabilization setup. The PID is sent to an in house lock box shown in reference[78], because this design had a high voltage operational amplifier that was discontinued we retrofitted the board to accommodate an apex PA441DW amplifier. The ramp of this custom ramp box is seen in the figure 3.3.

3.4 Cavity Cooling and Readout

Since the two beams are locked to the same reference cavity their coupling of the fundamental mode in the experimental cavity occurs as displayed in figure 3.3 and figure 3.4. For cavity assisted cooling the cavity cooling beam needs to be red detuned to carry away energy from the center of mass motion of the nanosphere along the cavity axis[11]. In order to detune the cooling beam we deploy two AOMs to change the frequency by the required amount as seen in figure 3.1. First there is a single pass through the first AOM then a double pass through the second AOM. As seen in figure 3.4 the red trace of the cooling beam is red detuned from the black trapping beam.

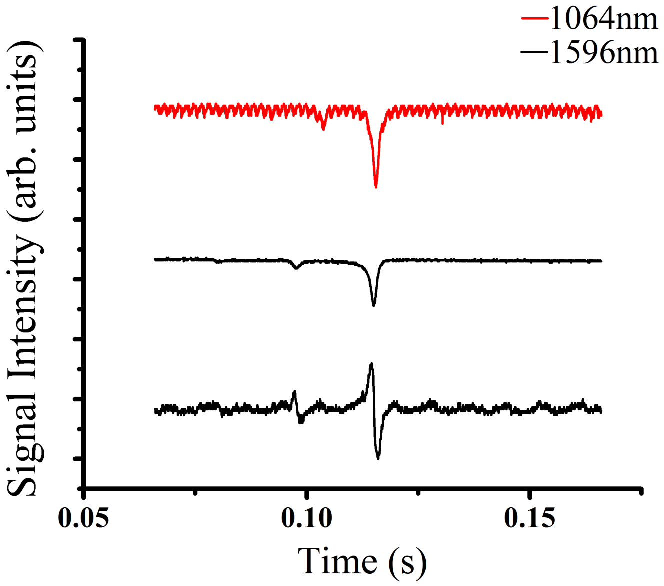

Figure 3.4: A shorter ramp of the piezo in the experimental cavity that shows in more detail the reflection signals from both the 1064 nm laser and the 1596 nm laser along with the demodulated signal of the 1596 nm laser.

The center-of-mass motion of the nano-sphere along the cavity axis modulates the phase of the cooling beam through the optomechanical coupling. In our case, we look at the reflected signal of the 1064 nm cooling beam and demodulate the signal with a commercial lock-in amplifier. One can see the signal readout in figure 3.4 as the lower black time trace.

3.5 Current Combined Cavity-Dual Beam Standing Wave System State

We have been successful loading the cavity optical standing wave trap, using the same method mentioned in section 2.2.

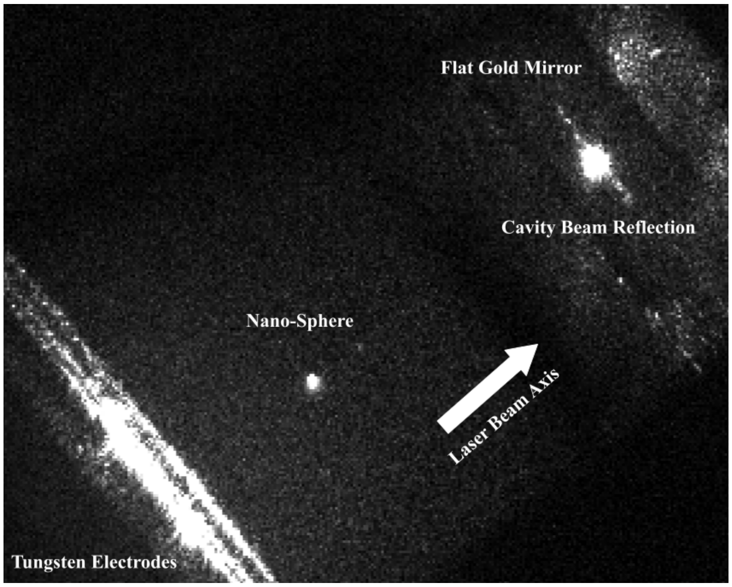

Figure 3.5: Image of the scattered cooling laser incident on a nano-sphere trapped inside the optical standing wave trap. This standing wave is created by the experimental optical cavity.

Because of the better trap depth of the dual beam optical standing wave trap, we have recently attempting the alignment and overlap of the two standing wave optical traps: the dual beam trap, and the cavity trap. To do this we are using a ~ 120 μm pinhole at approximately 25° angle from the dual beam axis. The stability of the dual beam standing wave optical trap would help us in accurately placing the nano-sphere in the cavity trapping and cooling beam. After first aligning the lasers into the cavity to achieve maximal loss in the reflection signal on resonance, we move one to trying to place the foci of the dual beam trap equidistant from the cavity standing wave focus. Even with multiple attempts involving clumps of nano-spheres and single nano-spheres, the amount of light scattered to our quadrant detectors from the 1596 nm cavity trapping laser is still on the order of .1% of the light scattered by the 1064 nm dual beam standing wave trap. One can see some experimental data for the intensity ratio for multiple trials in figure 3.6. This indicates that the two traps overlap is poor. We are currently developing an improved alignment strategy outlined in the next chapter.

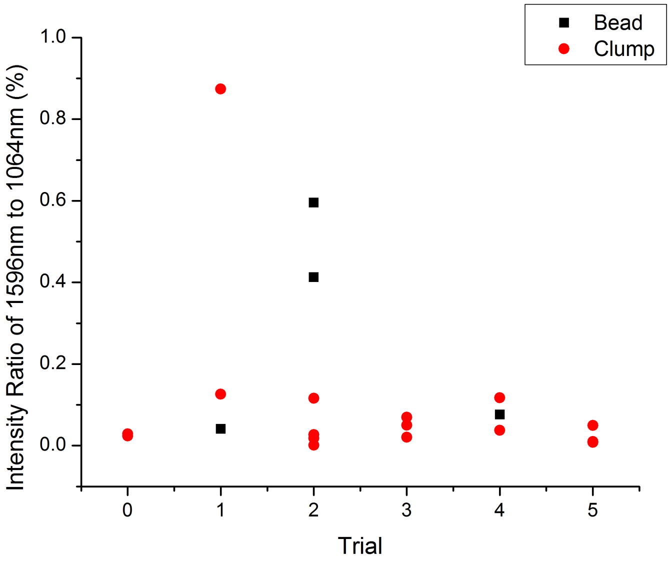

Figure 3.6: Intencity ratio in percent between the 1064 nm trapping light and the 1596 nm cavity trap; image from reference[79].

Chapter 4

Future Work

We believe that with improved imaging, better vacuum, and other system developments we will reach the predicted sensitivities required to test deviations from Newtonian gravity on a micron scale and improve bounds by several orders of magnitude. We plan to improve our imaging limits by improving the laser noise in the optical trapping lasers. Achieving higher vacuum by including an ion trap into the system will push the minimum detectable force even further. A redesign the dual beam optical standing wave trap using optical fibers is underway, allowing us to align the two optical standing wave traps *in situ*. Finally we can integrate a newly designed Invar experimental cavity that will reduce the thermal fluctuations in the cavity lowering noise in the system.

4.1 Imaging Limits

To characterize the noise associated with our signal from the quadrant photodectors (QPD), we must take into account three different types of noise: Johnson, other electronics noise, photon shot, and laser noise. These and non-conservative scattering cause heating of the fused silica nano-sphere in the dual beam optical standing wave trap. With a measured heating rate of 0.4 s^{-1}[42] we can assess the extent of heating due to the noise from the laser.

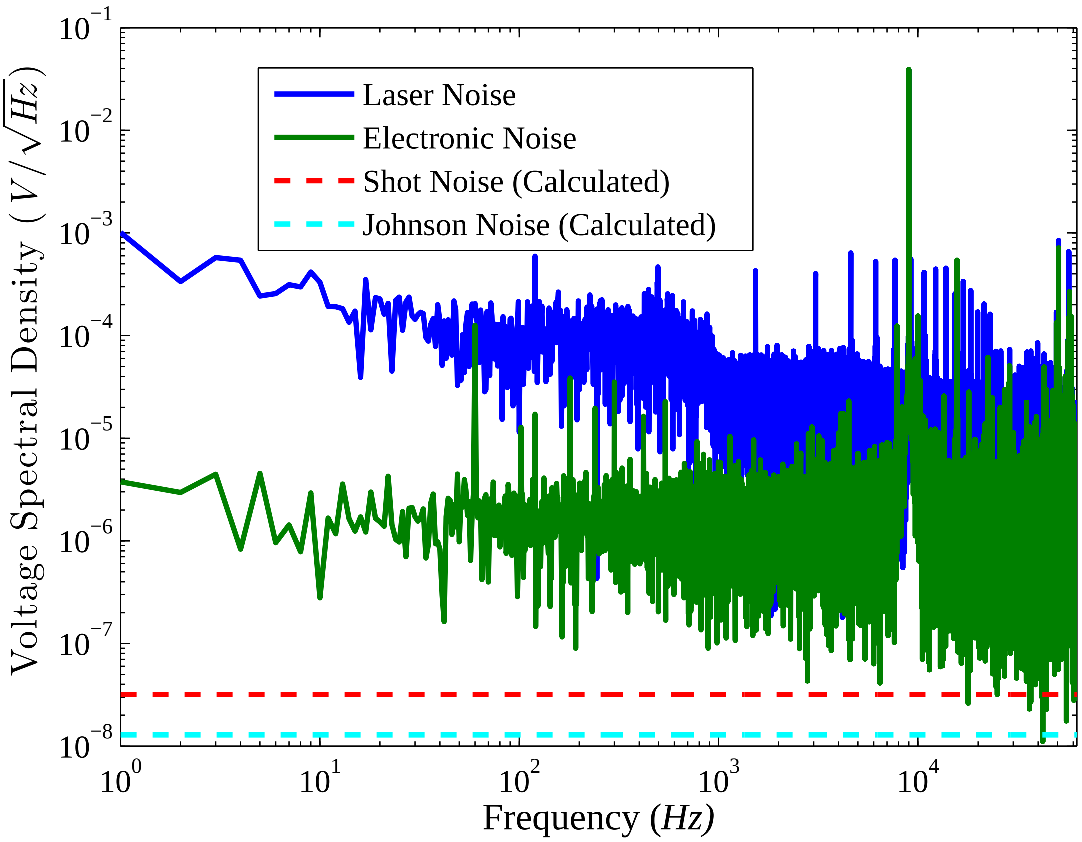

Figure 4.1: Voltage spectrum shown with 1064 nm laser incident to a quadrant photodetector(blue), laser blocked to show the dark current of the detector(green), calculated photon shot(red), and Johnson noise(cyan). The laser is at 65% driving current, corresponding to 1.37 W, after a 50/50 beam-splitter and neutral density filters with an OD = 3.6, the power is attenuated to 70 μW and focused with a 500 mm lens.

4.1.1 Johnson Noise

As you change the resistance or temperature of an amplifier circuit, one expects to see noise called Johnson noise.[80] First characterized by J.B. Johnson in the 1920's, the expected voltage from the this particular noise is:

$$V = \sqrt{4k_bTbR}\,[81] \tag{4.1}$$

where T is the temperature of the circuit, R is the amplifying resistance, b is the bandwidth, and k_b is the Boltzmann constant. The Johnson noise in our system is displayed as the dotted cyan line in figure 4.1, assuming a temperature of 300 K and a resistor value of 10K Ohms, corresponding to the transimpedance amplifier resistor on the quadrant photodetector.

4.1.2 Photon Shot Noise

Due to the quantum nature of light and the noise associated with the "randomness" of the number of incident photons, shot noise is also introduced. Shot noise was introduced by Walter H. Schottky in the 1910's and expounded in the 1920's[82]. Schottky's shot noise is characterized in current but with Ohm's Law we can write the voltage from shot noise as:

$$V = \sqrt{2e\eta P_0 bR^2}\,[81] \tag{4.2}$$

here e is the charge of a single electron, η is the responsivity, and P_0 is the incident power. The product of responsivity and Power equal current ($\eta P_0 = I$) which helps match Schottky's functional form of shot noise.

4.1.3 Laser Intensity Noise

The laser intensity noise occurs from noise in the laser power supply and laser pointing noise. The heating rate Γ_{int} for the laser intensity noise can be written as:

$$\Gamma_{int} = \pi^2 \nu_{tr}^2 S(2\nu_{tr})\,[83] \tag{4.3}$$

therefore the heating rate constant is dependent of the frequency of the trap (ν_{tr}) and the value at twice the trap frequency in the one-sided power spectrum of the fractional intensity noise, for our system $S(2\nu_{tr}) \approx 0.5Hz^{-1}$. Since it is a fractional intensity noise spectrum and the voltage on our detector is proportional to intensity, we calculate $S(2\nu_{tr})$ by looking at the average of the voltage 1 KHz around $2\nu_{tr}$ and then divide by the DC level of the detector. Our trap frequency is ~5000 Hz, which corresponds to a heating rate of ~15 $\times 10^{-3}\mathrm{s}^{-1}$. This is a rate for the increase of the energy by a factor e. This suggests that the majority of the heating is due to non-conservative scattering heating.

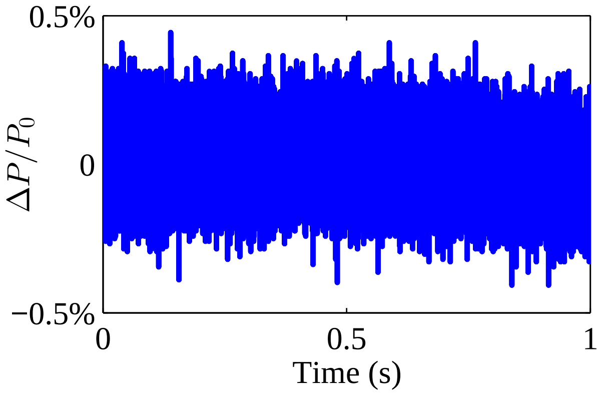

Figure 4.2: Typical Relative Power Noise from Intensity fluctuations.

The total Power($P(t)$) has some time dependent noise associated with it as shown here:

$$P(t) = P_0 + \Delta P(t) \tag{4.4}$$

Here $P(t)$ is the total power of the laser, P_0 is the mean output power, and $\Delta P(t)$ is the Power intensity noise. Figure 4.2 shows the relative time dependent power fluctuations for a 1 s or $\Delta P(t)/P_0$.

To see what noise to due to laser pointing we could use a lateral effect position-sensing detector. A lateral effect position-sensing detector is a quadrant photodector without separation between the four quadrants. Using the sum of the quadrant we could divide the intensity noise due to fluctuations and isolate the noise due to laser pointing. In order to mitigate the noise caused by laser fluctuations we could take the voltage of the signal from the sum and then divide each measured voltage. This gives us some way of dividing out the laser intensity noise on the lateral effect position-sensing detector. This analysis is not included in this thesis. The energy doubling heating due to laser pointing is:

$$\Gamma_{pointing} = \pi^2 \nu_{tr}^2 \frac{S(\nu_{tr})}{\langle x^2 \rangle} \, [83] \tag{4.5}$$

where $\langle x^2 \rangle$ is the mean square position of the nano-sphere in the trap.

4.2 Higher Vacuum

With improved imaging we will push the noise floor of our measurement even further. At that point, another improvement we can make is to push the vacuum of the system even further. We have in place an ion pump that, will be attached to the system to help us reach higher vacuum. The minimum detectable force mentioned earlier was written as:

$$F_{min} = S_{f_0}^{1/2} b^{1/2} = \sqrt{\frac{4k_b T b k}{\omega_0 Q}} \tag{4.6}$$

this equation can be rewritten using the damping rate applied to the nano-sphere.

$$F_{min} = \sqrt{4k_b T m \Gamma_m b}\,[43] \tag{4.7}$$

where $\Gamma_m = 16P/(\pi\rho v r)$ is the damping rate of a sphere with radius r, density ρ, in a gas medium of pressure P, and mean speed v. The important point is that $F_{min} \propto \sqrt{P}$, therefore the additional reduction of the pressure due to the ion pump can help reduce the F_{min} by ∼2 orders of magnitude.

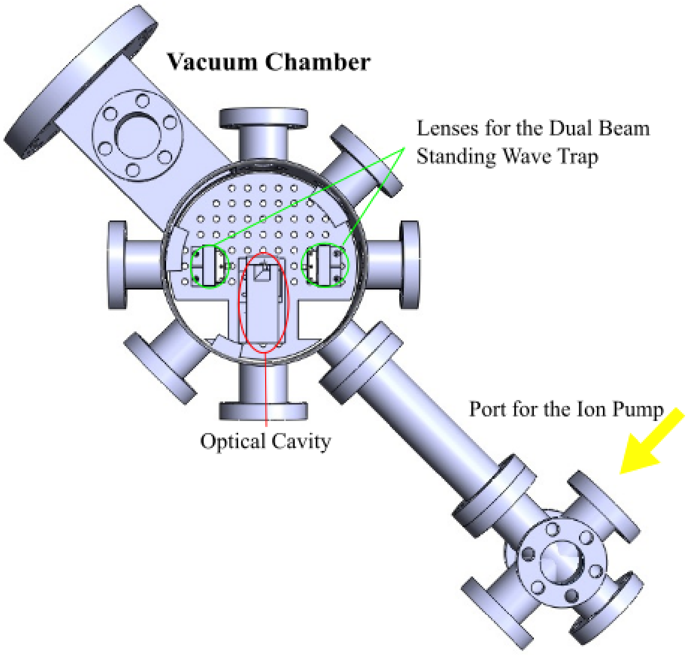

Figure 4.3: The vacuum chamber rendering in Solidworks. The yellow area indicates the port where the ion pump will be connected.

A Solidworks rendering of our vacuum system is shown in figure 4.3 at the cross the Ion pump was connected to the port indicated by the yellow arrow. In order to make the vacuum system feasible the Ion pump will need to have a valve somewhere between that port and the Ion pump. The valve will allow us to cycle between low and high vacuum, and keep the Ion pump powered.

4.3 Dipole Fiber System

Experimentaly we have seen some difficulty in overlapping the two optical standing wave traps. One solution would be an *in-situ* motion controled stategy to help optimize the two trap's overlap. This would require an overhaul of one of the two system, and for motion control of an optical trap we believed that optical fibers would be a necessary addition. Below in is a Solidworks rendering on an assembly involving three Newport AG-LS25 stages[84] with some custom assembling brackets, and a long lever arm. On the lever are there are two kinematic mirror mounts[85] used as fiber coupling mounts lens tubes with collimating lenses followed by focusing lenses to create the movable dual beam optical standing wave trap.

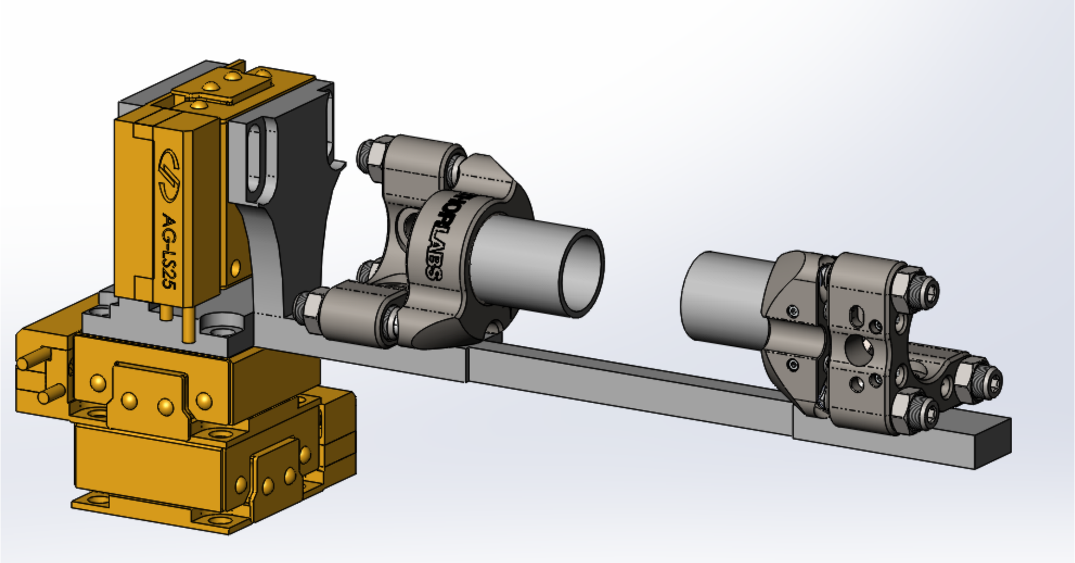

Figure 4.4: Assembly of Newport motion controlling stages connected via custom in house brackets. A lever arm with two kinetic mirror mounts repurposed as fiber coupling mounts is attached. With custom lens tubes inside the kinetic mounts we will create an optical standing wave trap between them.

As seen in other experimental setups[30] the ability to move an optically levitated nano-sphere is possible and may help us to effectively load the optical standing wave cavity trap and reach our experimental goal of overlap of the two standing optical wave traps. Ultimately helping us measure any non-Newtonian gravity like forces on the micron scale.

4.4 Invar Optical Cavity

Although the dominant noise in the system is due to laser and electronic noise, another improvement in the cavity system is to replace the aluminum cavity that is made from three pieces, to a single continuous Invar cavity. The current cavity is construction of three pieces can be seen in figure 4.5. The mirrors attached via vacuum compatible epoxy on the inside, the flat gold mirror at the inset and the round IR coated mirror near the circular aperture. The third piece is the cavity footing at the bottom of the cavity, this provides stability and height.

On top of the cavity there is a copper spool wrapped in copper wire that acts as a heating coil for the cavity. Along with a thermistor and a temperature controlling digital PID circuit[86], we heat the coil to keep the temperature of the cavity constant. This helps the cavity to maintain its length. Therefore adding to the stability of the cavity coupling of the 1064 nm cooling laser and the 1596 nm trapping laser.

The coefficient of linear thermal expansion of Invar is approximately 1.5 parts per million (ppm) where Aluminum's is 21 to 24 ppm.[87] That is 14 - 16 times less expansion per degree C. Also to improve the mechanical stability the Invar the cavity will be singularly carved using precision wire electrical discharge machining (EDM). With the improved stability of the cavity; the clamp, copper spool and thermistors attached to the cavity become superfluous and will free four electrical feedthroughs into the chamber.

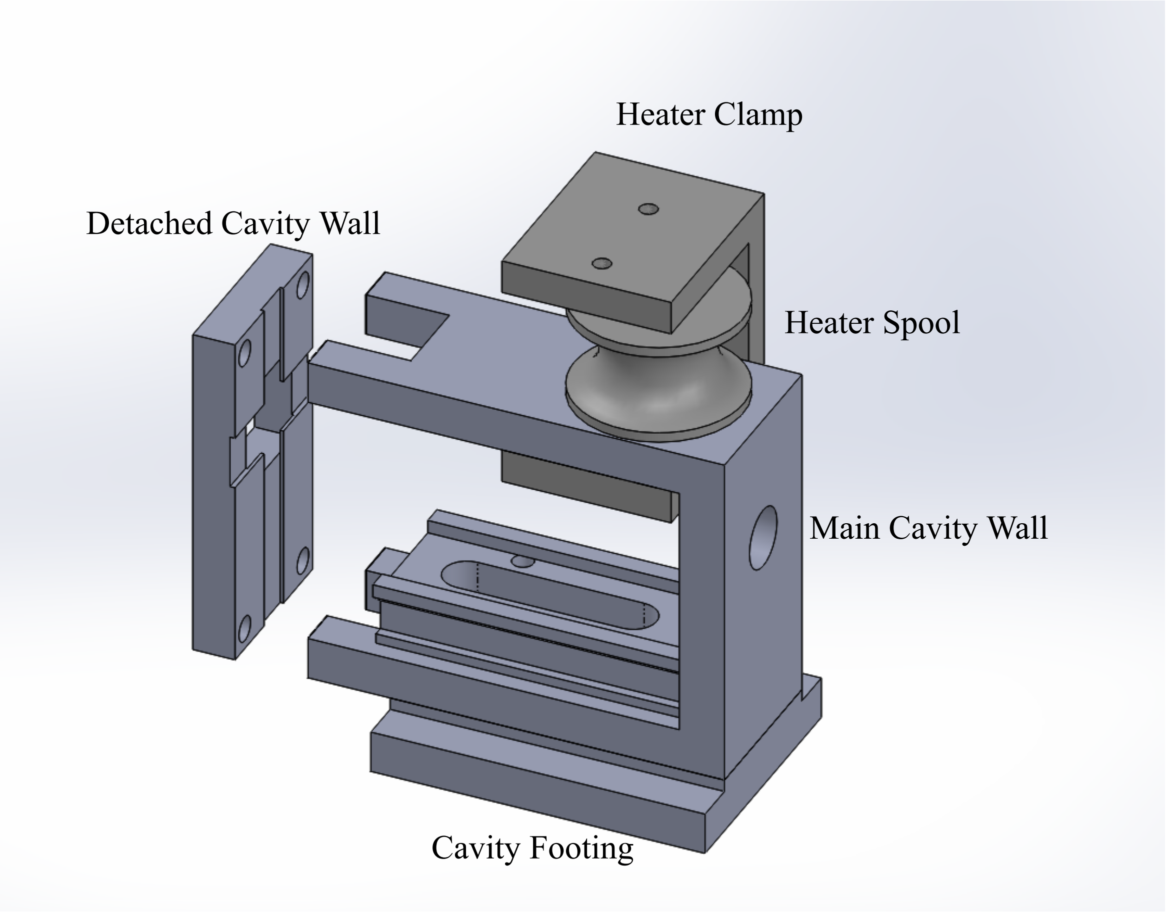

Figure 4.5: The cavity is constructed of three aluminum pieces separated here to show the two of the three pieces. In order to control the temperature of this cavity and ease the noise of thermal expansion there is a copper heater spool clamped to the cavity with copper heating wire wrapped around as a heating element. With a thermistor and a PID controller we feedback to the heater to control the temperature of the cavity.

Appendix A

Matlab Analysis

The following Matlab codes file name is PhaseWiseAvgWithPaddingBinDataModified.m. This file retrieves data from our external hard drive, performs a padded fft, a phasewise average, and saves the voltage spectral density of the recorded data in a particular folder. The following comments in green act as a code header, and give an overview of the file, its original author, its last modification, who last modified the file, and relevant dates.

```
%************************************************************
% Description: Takes Binary Data, does a Phase wise Average,*
% writes text file with the real part and imaginary part,   *
% phase, amplitude, and plots fft and saves.  Runs according*
% to bead number.                                           *
%                                                           *
% Created by: Gambhir Ranjit                                *
%                                                           *
% Last modification description:  fixed a double counting   *
% for the first file in the averaging. changed an           *
% if-end-if-else-end  to a if-elseif-else-end structure.    *
% Changes made to lines 156, 246                            *
%                                                           *
% Last Modified by: Mark Cunningham                         *
% Date Modified: 02/25/2016                                 *
%************************************************************
```

When I inherited the analysis role, this type of code description was not in any files in our analysis suite. It was implemented to help keep files versionized and organized.

This particular file starts by clearing any legacy data.

```
%% Fresh start
close all;
clear all;
iStart = 0;
```

—

Since our data is organized by the date folder, the following code asks you to select a certain data file. Then taking the bead number assigned to the file using regular expressions, it makes a list of all the other files with the same bead number. Later the program will prompt the user if he/she would like to iterate through the list. This works because all of the data file follow the same naming convention.

```
%%!User selects a folder of specific bead  to run then all files in
% date folder are crunched!!!!!!!!!!!!!!!!!!!!!!!!!!!!!!!!!!!!!!!!!
file = uigetdir('E:\');
date = char(regexp(file, '... .., ....(?=\\)', 'match'));
beadNumber = char(regexp(file, 'bead(\d+)', 'match'));
drive = char(regexp(file, '.\:\\', 'match'));

Fs = 250000; % sampling frequency

% by bead number
cd(strcat(drive,date,'\'));
files = char(regexp(file, 'Data.*bead(\d+)', 'match'));
list = ls('Data_*');
cnt = 1;
for i = 1:size(list,1)
    if strcmp(char(regexp(list(i,:),'bead(\d+)','match')),beadNumber)
        list2(cnt,:)=list(i,:);
        cnt = cnt+1;
    end
end
filedata = cellstr(list2);
```

If you would like you could comment out the above code and just hard code a file name or a list of file names to iterate.

```
%!!!!!!!!!!!!!!!!!!!!!!!!!!!!!!!!!!!!!!!!!!!!!!!!!!!!!!!!!!!!!!!!!!!!

% @@@@@@@@@@@@@@@@list of specific files to run@@@@@@@@@@@@@@@@@@@@@@
% fullfileName = {
%     'Data_Wed, Dec 10, 2014_7000_bead2_thermal0_60Vp             ';
% };
% filedata = cellstr(fullfileName);
```

```
% @@@@@@@@@@@@@@@@@@@@@@@@@@@@@@@@@@@@@@@@@@@@@@@@@@@@@@@@@@@@@@@@@@@
```

Each data file name has a frequency corresponding to the resonant frequencies of interest. This snippet of code with get those frequencies for use later in creating frequency specific data files.

```
%%~~~GET the frequencies of interest~~~~~~~~~~~~~~~~~~~~~~~~~~~~~~~~
fourDigit = regexp(filedata{1}, '(\d{4})', 'match');
freq(1) = str2double(fourDigit{2});
cnt = 1;

for i = 1:length(filedata)
    % gets off resonant driving frequency
    fourDigit = regexp(filedata{i}, '(\d{4})', 'match');
    freqc = str2double(fourDigit{2});
    if freqc ~= freq(cnt)
        cnt = cnt+1;
        freq(cnt)=freqc;
    end
end
%  freq = [1058, 1178, 7000];
%~~~~~~~~~~~~~~~~~~~~~~~~~~~~~~~~~~~~~~~~~~~~~~~~~~~~~~~~~~~~~~~~~~~~
```

The following code prompts the user to choose whether to execute all the files in the current directory folder of the same nano-sphere name or not. Also the user is given the choice to add any more frequencies of interest that are not listed in the file names.

```
bybead = input('Would you like to crunch the whole bead? y/n:  '...
, 's');
freqcheck = input('Would you like to specify more frequencies? y/n: ...
','s');
if bybead ~= 'y'
    filedata = cellstr(regexp(file, 'Data_.*$','match'));
end
```

The next segment of code uses a for loop to iterates through the list of file names that the user has decided to run. The following if statements ensure that we don't repeat computation. Just a note, through the remaining code in the appendix the tabs have been removed to help the code fit on the page.

```
for j = 1:length(filedata)
    pName = strcat(drive,date,'\',filedata{j});
    cd(pName);
    pathName = char(strcat(drive,'DataOutput\PhaseWAnalysis\',...
    date,'\'));
    if ~exist(pathName,'dir')
        mkdir(pathName);
    end
    if exist(strcat(pathName,filedata{j},'AvgrealImag.txt'),'file')==0
    if ~strcmp(char(regexp(filedata{j},'pos_shift','match')),...
    'pos_shift')
    if ~strcmp(char(regexp(filedata{j},'slowpumping','match')),...
    'slowpumping')
    if ~strcmp(char(regexp(filedata{j},'fastpumping','match')),...
    'fastpumping')
    if ~strcmp(char(regexp(filedata{j},'beadloss','match')),'beadloss')
```

The data we collect is a .bin file consisting a single second of data. We collect these file continuously for long averaging times up to 10^5 s, meaning there are that many .bin files needing to be averaged for that data run. A typical data run is about 100 s. Because of the variance in data run times, this snippet will find the bandwidth of our measurement by checking the number of .bin files. That number is saved and used by iterating for loops later.

```
 %%% finds number of bin files is data folder@@@@@@@@@@@@@@@@@@@@@@@
list = cellstr(ls('*.bin'));
if ~isempty(list)
iStop = length(list)-1;
 disp(strcat('Currently running Data file: ',filedata{j}))
%%% @@@@@@@@@@@@@@@@@@@@@@@@@@@@@@@@@@@@@@@@@@@@@@@@@@@@@@@@@@@@@@@
```

If the user previously chose to add new frequencies to add to the frequency specific data collection, the next if statement gets the data from a few files, performs an fft, and displays the voltage spectrum to the user. The user views the spectrum and can add frequencies in a comma separated list.

```
                    %% frequency specify
if freqcheck == 'y'
    for l = iStart:iStart+2
        fName = strcat('\Data',num2str(l),'.bin');
        fileNameIn = char(strcat(pName, fName));
        fid = fopen(fileNameIn,'r');
```

```
        Y= fread(fid,[5,250000],'double'); % file size here
        fclose(fid);
        y = Y';

        x1 = y(1:125000)';      % file size changes.
        x2 = y(125001:250000)'; %
        x3 = y(250001:375000)'; %
        x4 = y(375001:500000)';%
        L = length(x1);
        xRaw = linspace(1,L,L);
        xn = xRaw;

        if L > 125000
            xRaw = xRaw(1:length(xRaw)-1);
            x1 = x1(1:length(xRaw)-1);
            x2 = x2(1:length(xRaw)-1);
            x3 = x3(1:length(xRaw)-1);
            x4 = x4(1:length(xRaw)-1);
            xn = xRaw(1:(L-1));
        end

        if l == iStart
            LCrossIn = 0;
        else
            LCrossIn = LCrossOut;
        end
        [signalshort, xPlot, ch1short, ch2short,ch3short, LCrossOut]...
            = properphasefft(x4,x1,x2,x3, LCrossIn, l-iStart);
        length(signalshort);

        if l == iStart
            NFirstSignal = length(signalshort);
            NPadding = 1;
            NForPad = Fs - length(signalshort) - NPadding;
        end

        [sfPlot, sPlot, sPhi, sReal, sImag] = ...
         doFFTNPad(signalshort, Fs, NForPad);
         [ch1fPlot, ch1Plot, ch1Phi, ch1Real, ch1Imag]...
             = doFFTNPad(ch1short, Fs, NForPad);
         [ch2fPlot, ch2Plot, ch2Phi, ch2Real, ch2Imag]...
             = doFFTNPad(ch2short, Fs, NForPad);
         [ch3fPlot, ch3Plot, ch3Phi, ch3Real, ch3Imag]...
             = doFFTNPad(ch3short, Fs, NForPad);

        if l == iStart
            sRealNew = sReal;
            sImagNew = sImag;
            ch1RealNew = ch1Real;
            ch1ImagNew = ch1Imag;
            ch2RealNew = ch2Real;
            ch2ImagNew = ch2Imag;
```

```
            ch3RealNew = ch3Real;
            ch3ImagNew = ch3Imag;
        elseif length(sReal)==length(sRealNew)
            sRealNew = sRealNew + sReal;
            sImagNew = sImagNew + sImag;

            ch1RealNew = ch1RealNew + ch1Real;
            ch1ImagNew = ch1ImagNew + ch1Imag;

            ch2RealNew = ch2RealNew + ch2Real;
            ch2ImagNew = ch2ImagNew + ch2Imag;

            ch3RealNew = ch3RealNew + ch3Real;
            ch3ImagNew = ch3ImagNew + ch3Imag;
        else
            disp('what the what!!!Mark');
        end
        fclose all;
    end
    fr = sfPlot;
%     fr = linspace(0,(length(sRealNew)-1), length(sRealNew));
    zAvg = [fr; sRealNew; sImagNew; ch1RealNew; ch1ImagNew;...
        ch2RealNew; ch2ImagNew; ch3RealNew; ch3ImagNew];

    cFFT_Ch1 = complex(zAvg(4,:), zAvg(5,:))/(i+1);
    figure(6);
    plot(zAvg(1,:), 2*abs(cFFT_Ch1));
    loglog(zAvg(1,(10:length(fr))), 2*abs(cFFT_Ch1(10:length(fr))));
    xlim([10,length(fr)])


    cFFT_Ch2 = complex(zAvg(6,:), zAvg(7,:))/(i+1);
    figure(7);
    plot(zAvg(1,:), 2*abs(cFFT_Ch2));
    loglog(zAvg(1,(10:length(fr))), 2*abs(cFFT_Ch2(10:length(fr))));
    xlim([10,length(fr)])


    cFFT_Ch3 = complex(zAvg(8,:), zAvg(9,:))/(i+1);
    figure(8);
    plot(zAvg(1,:), 2*abs(cFFT_Ch3));
    loglog(zAvg(1,(10:length(fr))), 2*abs(cFFT_Ch3(10:length(fr))));
    xlim([10,length(fr)])

    freqs = ...
input('Which frequencies would you like to add.  separate ...
frequencies by just "," (no space)','s');
    freqlist = regexp(freqs, ',', 'split');

    for m = 1:length(freqlist)
        freq(length(freq)+ 1) = str2double(freqlist{m});
    end
```

```
end
```

We will see a lot of that code again, and it will be explained later in more detail. Following that if statement, there is an iterating for loop that will execute the following code for all of the .bin files in the folder. This following snippet of code opens the files. There are a few commented lines present in case we decide to change the sampling frequency of our measurement.

```
%% Opening file to read in data *******************************
fName = strcat('\Data',num2str(i),'.bin');
fileNameIn = char(strcat(pName, fName));

% ---------------------------------------------------------- %

fid = fopen(fileNameIn,'r');
Y= fread(fid,[4,250000],'double'); % file size changes
fclose(fid);
y = Y';

x1 = y(1:125000)';      % file size changes.
x2 = y(125001:250000)'; %
x3 = y(250001:375000)'; %
x4 = y(375001:500000)';%

% x1 = y(1:250000)';          % file size changes
% x2 = y(250001:500000)';     %
% x3 = y(500001:750000)';     %
% x4 = y(750001:1000000)';    %
L = length(x1);
xRaw = linspace(1,L,L);
xn = xRaw;

% xRaw = inDataRead{1}(1:length(xRaw)-1);
% x1 = inDataRead{2}(1:length(xRaw)-1);
% x2 = inDataRead{3}(1:length(xRaw)-1);
% x3 = inDataRead{4}(1:length(xRaw)-1);
% defines # of samples in a single set

if L > 125000
    xRaw = xRaw(1:length(xRaw)-1);
    x1 = x1(1:length(xRaw)-1);
    x2 = x2(1:length(xRaw)-1);
    x3 = x3(1:length(xRaw)-1);
    x4 = x4(1:length(xRaw)-1);
    xn = xRaw(1:(L-1));
end
```

The next two peices of code makes sure that the phase of the bin files match, to ensure an in phase fft is done.

```
%% %%%%%%%%%%%% Rectangular Windowing to have fixed Phase%%%%%%

if i == iStart
    LCrossIn = 0;
else
    LCrossIn = LCrossOut;
end

[signalshort, xPlot, ch1short, ch2short,ch3short, LCrossOut]...
    = properphasefft(x4,x1,x2,x3, LCrossIn, i-iStart);
length(signalshort);


%% %%%%%%%%%%%%%%%% ZeroPadding %%%%%%%%%%%%%%%%%%%%%%%%%%%%%%%
if i == iStart
    NFirstSignal = length(signalshort);
    NPadding = 1;
    NForPad = Fs - length(signalshort) - NPadding;
end
```

The code is repeated for each channel: signal, channel 1, channel 2, and channel 3. It is commented to help explain each line.

```
indCloseToFreqS = find(abs(sfPlot-freq(k)) == min(abs(sfPlot-freq(k))));
% finds the closest frequency to driving frequency
sAmp = sPlot(indCloseToFreqS);
% finds the peak within the range of + or - 2 Hz
indMaxSig = indCloseToFreqS;
% finds the index where the highest peak occurs
SignalReal = sReal(indMaxSig); % real part at the peak position
SignalImag = sImag(indMaxSig); % imaginary part at the peak position
freqSig = sfPlot(indMaxSig); % frequency at the peak position
sPhase = sPhi(indMaxSig); % phase at the peak position
```

The next example appends a frequency specific file with the data values listed in the first comment. This file is the frequency specific file mentioned earlier. With this information we can create scatter plots and long averaging force measurements over time shown in section 2.4.

```
%% This writes the data as (frequency,amplitude, phase, real,
```

```
% imaginary) for signal, channel 1, 2, and 3 respectively%
z = [freqSig, sAmp, sPhase, SignalReal, SignalImag, freqch1,...
    ch1Amp, ch1Phase, channel1Real, channel1Imag, freqch2, ch2Amp,...
    ch2Phase, channel2Real, channel2Imag, freqch3, ch3Amp, ch3Phase,...
    channel3Real, channel3Imag];

% Saves data as a text file in PhaseWAnalysis folder$$$$$$$
if sAmp>0.00
    if length(z) == 20
     fileNameOut = ...
     strcat(pathName,filedata{j},num2str(freq(k)),...
     'realImag.txt');
        fID = fopen(fileNameOut,'a');
     fprintf(fID,'%f\t %f\t %f\t %f\t %f\t %f\t %f\t %f\t ...
     %f\t %f\t %f\t %f\t %f\t %f\t %f\t %f\t %f\t %f\t %f\t ...
     %f\r\n',z);
    else
        disp(strcat('error in finding the point...
         precisely in the file',num2str(i)))
    end
end
%$$$$$$$$$$$$$$$$$$$$$$$$$$$$$$$$$$$$$$$$$$$$$$$$$$$$$$$$$$$
```

The following is the averaging of all the data over the whole spectrum.

```
if i == iStart
sRealNew = sReal;
sImagNew = sImag;
ch1RealNew = ch1Real;
ch1ImagNew = ch1Imag;
ch2RealNew = ch2Real;
ch2ImagNew = ch2Imag;
ch3RealNew = ch3Real;
ch3ImagNew = ch3Imag;
elseif length(sReal)==length(sRealNew)
sRealNew = sRealNew + sReal;
sImagNew = sImagNew + sImag;

ch1RealNew = ch1RealNew + ch1Real;
ch1ImagNew = ch1ImagNew + ch1Imag;

ch2RealNew = ch2RealNew + ch2Real;
ch2ImagNew = ch2ImagNew + ch2Imag;

ch3RealNew = ch3RealNew + ch3Real;
ch3ImagNew = ch3ImagNew + ch3Imag;
else
disp('what the what!!!#@$!@!!');
end
%% !!!!!!!!!!!!!!!!!!!!!!!!!!!!!!!!!!!!!!!!!!!!!!!!!!!!!!!!!!!!
fclose all;
```

Here we save the averaged file over the entire spectrum. This file is used for displaying cooling and helping with force calibration. Also the plot of the voltage spectral density of each channel is saved. Here only the signal channel is shown.

```
%% Saves the averaged data as a text file@@@@@@@@@@@@@@@@@@@@@@@@@@
fr = sfPlot;
% fr = linspace(0,(length(sRealNew)-1), length(sRealNew));
zAvg = [fr; sRealNew; sImagNew; ch1RealNew; ch1ImagNew; ch2RealNew;...
    ch2ImagNew; ch3RealNew; ch3ImagNew];
fileNameOutAvg = strcat(pathName,filedata{j},'AvgrealImag.txt');
fID = fopen(fileNameOutAvg,'w');
fprintf(fID,'%f\t %f\t %f\t %f\t %f\t %f\t %f\t %f\t %f\r\n',zAvg);
%@@@@@@@@@@@@@@@@@@@@@@@@@@@@@@@@@@@@@@@@@@@@@@@@@@@@@@@@@@@@@@@@@@

%% %%%%%%%%%%%%%%%%%%%Creates and Saves the Plots%%%%%%%%%%%%%%%%%%
pathNamefig = strcat(pathName,'figures\',filedata{j},'\');
if ~exist(pathNamefig,'dir')
    mkdir(pathNamefig);
end

cFFT_S = complex(zAvg(2,:), zAvg(3,:))/(iStop-iStart+1);
hf5 = figure(5);
plot(zAvg(1,:), 2*abs(cFFT_S));
loglog(zAvg(1,(10:length(fr))), 2*abs(cFFT_S(10:length(fr))));
xlim([10,length(fr)])
saveas(hf5,strcat(pathNamefig,'Signal'),'fig');
```

The frequency specific files and the averaged files reduce terabytes of data to meaningful consumable data. Also this averaging code is the formatting springboard for multiple files that perform many other different computations.

Bibliography

[1] A. Ashkin, "Acceleration and trapping of particles by radiation pressure," *Phys. Rev. Lett.*, vol. 24, pp. 156–159, Jan 1970.

[2] A. Ashkin and J. M. Dziedzic, "Optical levitation by radiation pressure," *Applied Physics Letters*, vol. 19, no. 8, pp. 283–285, 1971.

[3] A. Ashkin, "Atomic-beam deflection by resonance-radiation pressure," *Phys. Rev. Lett.*, vol. 25, pp. 1321–1324, Nov 1970.

[4] J. E. Bjorkholm, A. Ashkin, and D. B. Pearson, "Observation of resonance radiation pressure on an atomic vapor," *Applied Physics Letters*, vol. 27, no. 10, pp. 534–537, 1975.

[5] A. Ashkin, "Trapping of atoms by resonance radiation pressure," *Phys. Rev. Lett.*, vol. 40, pp. 729–732, Mar 1978.

[6] A. Ashkin, J. M. Dziedzic, J. E. Bjorkholm, and Steven Chu, "Observation of a single-beam gradient force optical trap for dielectric particles," *Opt. Lett.*, vol. 11, no. 5, pp. 288–290, May 1986.

[7] A. Ashkin and J. M. Dziedzic, "Optical trapping and manipulation of viruses and bacteria," *Science*, vol. 235, no. 4795, pp. 1517–1520, 1987.

[8] A. Ashkin, J. M. Dziedzic, and T. Yamane, "Optical trapping and manipulation of single cells using infrared laser beams," *Nature*, vol. 330, pp. 769–771, 1987.

[9] A. Ashkin and J. M. Dziedzic, "Optical levitation in high vacuum," *Applied Physics Letters*, vol. 28, no. 6, pp. 333–335, 1976.

[10] A. Ashkin, "Optical trapping and manipulation of neutral particles using lasers," *Proceedings of the National Academy of Sciences*, vol. 94, no. 10, pp. 4853–4860, 1997.

[11] D. E. Chang, C. A. Regal, S. B. Papp, D. J. Wilson, J. Ye, O. Painter, H. J. Kimble, and P. Zoller, "Cavity opto-mechanics using an optically levitated nanosphere," *Proceedings of the National Academy of Sciences*, vol. 107, no. 3, pp. 1005–1010, 2010.

[12] Vijay Jain, Jan Gieseler, Clemens Moritz, Christoph Dellago, Romain Quidant, and Lukas Novotny, "Direct measurement of photon recoil from a levitated nanoparticle," *Phys. Rev. Lett.*, vol. 116, pp. 243601, Jun 2016.

[13] J. Millen, P. Z. G. Fonseca, T. Mavrogordatos, T. S. Monteiro, and P. F. Barker, "Cavity cooling a single charged levitated nanosphere," *Phys. Rev. Lett.*, vol. 114, pp. 123602, Mar 2015.

[14] Tongcang Li, Simon Kheifets, and Mark G. Raizen, "Millikelvin cooling of an optically trapped microsphere in vacuum," *Nat Phys*, vol. 7, pp. 527–530, 07 2011.

[15] Jan Gieseler, Bradley Deutsch, Romain Quidant, and Lukas Novotny, "Subkelvin parametric feedback cooling of a laser-trapped nanoparticle," *Phys. Rev. Lett.*, vol. 109, pp. 103603, Sep 2012.

[16] Jamie Vovrosh, Muddassar Rashid, David Hempston, James Bateman, Mauro Paternostro, and Hendrik Ulbricht, "Parametric feedback cooling of levitated optomechanics in a parabolic mirror trap," *J. Opt. Soc. Am. B*, vol. 34, no. 7, pp. 1421–1428, Jul 2017.

[17] Nikolai Kiesel, Florian Blaser, Uro Deli, David Grass, Rainer Kaltenbaek, and Markus Aspelmeyer, "Cavity cooling of an optically levitated submicron particle," *Proceedings of the National Academy of Sciences*, vol. 110, no. 35, pp. 14180–14185, 2013.

[18] Gambhir Ranjit, Cris Montoya, and Andrew A. Geraci, "Cold atoms as a coolant for levitated optomechanical systems," *Phys. Rev. A*, vol. 91, pp. 013416, Jan 2015.

[19] Andrew Geraci and Hart Goldman, "Sensing short range forces with a nanosphere matter-wave interferometer," *Phys. Rev. D*, vol. 92, pp. 062002, Sep 2015.

[20] James Bateman, Stefan Nimmrichter, Klaus Hornberger, and Hendrik Ulbricht, "Near-field interferometry of a free-falling nanoparticle from a point-like source," *Nature Communications*, vol. 5, Sep 2014.

[21] Oriol Romero-Isart, Mathieu L Juan, Romain Quidant, and J Ignacio Cirac, "Toward quantum superposition of living organisms," *New Journal of Physics*, vol. 12, no. 3, pp. 033015, 2010.

[22] Oriol Romero-Isart, "Quantum superposition of massive objects and collapse models," *Phys. Rev. A*, vol. 84, pp. 052121, Nov 2011.

[23] Asimina Arvanitaki and Andrew A. Geraci, "Detecting high-frequency gravitational waves with optically levitated sensors," *Phys. Rev. Lett.*, vol. 110, pp. 071105, Feb 2013.

[24] Alexander G. Krause, Martin Winger, Tim D. Blasius, Qiang Lin, and Oskar Painter, "A high-resolution microchip optomechanical accelerometer," *Nat Photon*, vol. 6, pp. 768–772, 11 2012.

[25] Tongcang Li, Simon Kheifets, David Medellin, and Mark G. Raizen, "Measurement of the instantaneous velocity of a brownian particle," *Science*, vol. 328, no. 5986, pp. 1673–1675, 2010.

[26] Andrew A. Geraci, Scott B. Papp, and John Kitching, "Short-range force detection using optically cooled levitated microspheres," *Phys. Rev. Lett.*, vol. 105, pp. 101101, Aug 2010.

[27] Martin Frimmer, Karol Luszcz, Sandra Ferreiro, Vijay Jain, Erik Hebestreit, and Lukas Novotny, "Controlling the net charge on a nanoparticle optically levitated in vacuum," *Phys. Rev. A*, vol. 95, pp. 061801, Jun 2017.

[28] P. Z. G. Fonseca, E. B. Aranas, J. Millen, T. S. Monteiro, and P. F. Barker, "Nonlinear dynamics and strong cavity cooling of levitated nanoparticles," *Phys. Rev. Lett.*, vol. 117, pp. 173602, Oct 2016.

[29] David Grass, Julian Fesel, Sebastian G. Hofer, Nikolai Kiesel, and Markus Aspelmeyer, "Optical trapping and control of nanoparticles inside evacuated hollow core photonic crystal fibers," *Applied Physics Letters*, vol. 108, no. 22, pp. 221103, 2016.

[30] Pau Mestres, Johann Berthelot, Marko Spasenovi, Jan Gieseler, Lukas Novotny, and Romain Quidant, "Cooling and manipulation of a levitated nanoparticle with an optical fiber trap," *Applied Physics Letters*, vol. 107, no. 15, pp. 151102, 2015.

[31] F. Ricci, R. A. Rica, M. Spasenovi, J. Gieseler, L. Rondin, L. Novotny, and R. Quidant, "Optically levitated nanoparticle as a model system for stochastic bistable dynamics," *Nature Communications*, vol. 8, pp. 15141, 2017.

[32] Muddassar Rashid, Tommaso Tufarelli, James Bateman, Jamie Vovrosh, David Hempston, M. S. Kim, and Hendrik Ulbricht, "Experimental realization of a thermal squeezed state of levitated optomechanics," *Phys. Rev. Lett.*, vol. 117, pp. 273601, Dec 2016.

[33] Levi P. Neukirch, Eva Von Haartman, Jessica M. Rosenholm, and A. Nick Vamivakas, "Multi-dimensional single-spin nano-optomechanics with a levitated nanodiamond," *Nature Photonics*, vol. 9, no. 10, pp. 653–657, 10 2015, Copyright - Copyright Nature Publishing Group Oct 2015; Last updated - 2016-02-23.

[34] Thai M. Hoang, Jonghoon Ahn, Jaehoon Bang, and Tongcang Li, "Electron spin control of optically levitated nanodiamonds in vacuum," *Nature Communications*, vol. 7, pp. 12250, 07 2016, Copyright - Copyright Nature Publishing Group Jul 2016; Last updated - 2016-07-23.

[35] Martin Frimmer, Jan Gieseler, and Lukas Novotny, "Cooling mechanical oscillators by coherent control," *Phys. Rev. Lett.*, vol. 117, pp. 163601, Oct 2016.

[36] Moser J., Guttinger J., Eichler A., Esplandiu M. J., Liu D. E., Dykman M. I., and Bachtold A., "Ultrasensitive force detection with a nanotube mechanical resonator," *Nat Nano*, vol. 8, pp. 493–496, 7 2013.

[37] C Doolin, P H Kim, B D Hauer, A J R MacDonald, and J P Davis, "Multidimensional optomechanical cantilevers for high-frequency force sensing," *New Journal of Physics*, vol. 16, no. 3, pp. 035001, 2014.

[38] Christoph Reinhardt, Tina Müller, Alexandre Bourassa, and Jack C. Sankey, “Ultralow-noise sin trampoline resonators for sensing and optomechanics,” *Phys. Rev. X*, vol. 6, pp. 021001, Apr 2016.

[39] Houxun Miao, Kartik Srinivasan, and Vladimir Aksyuk, “A microelectromechanically controlled cavity optomechanical sensing system,” *New Journal of Physics*, vol. 14, no. 7, pp. 075015, 2012.

[40] Gavartin E., Verlot P., and Kippenberg T. J., “A hybrid on-chip optomechanical transducer for ultrasensitive force measurements,” *Nat Nano*, vol. 7, pp. 509–514, 8 2012.

[41] R. A. Norte, J. P. Moura, and S. Gröblacher, “Mechanical resonators for quantum optomechanics experiments at room temperature,” *Phys. Rev. Lett.*, vol. 116, pp. 147202, Apr 2016.

[42] Gambhir Ranjit, Mark Cunningham, Kirsten Casey, and Andrew A. Geraci, “Zeptonewton force sensing with nanospheres in an optical lattice,” *Phys. Rev. A*, vol. 93, pp. 053801, May 2016.

[43] Gambhir Ranjit, David P. Atherton, Jordan H. Stutz, Mark Cunningham, and Andrew A. Geraci, “Attonewton force detection using microspheres in a dual-beam optical trap in high vacuum,” *Phys. Rev. A*, vol. 91, pp. 051805, May 2015.

[44] Nima ArkaniHamed, Savas Dimopoulos, and Gia Dvali, “The hierarchy problem and new dimensions at a millimeter,” *Physics Letters B*, vol. 429, no. 3, pp. 263 – 272, 1998.

[45] S. Dimopoulos and G.F. Giudice, “Macroscopic forces from supersymmetry,” *Physics Letters B*, vol. 379, no. 1, pp. 105 – 114, 1996.

[46] S. K. Lamoreaux, “Demonstration of the Casimir Force in the 0.6 to 6 μm Range,” *Physical Review Letters*, vol. 78, pp. 5–8, Jan. 1997.

[47] A. O. Sushkov, W. J. Kim, D. A. R. Dalvit, and S. K. Lamoreaux, “Observation of the thermal Casimir force,” *Nature Physics*, vol. 7, pp. 230–233, Mar. 2011.

[48] D. J. Kapner, T. S. Cook, E. G. Adelberger, J. H. Gundlach, B. R. Heckel, C. D. Hoyle, and H. E. Swanson, “Tests of the gravitational inverse-square law below the dark-energy length scale,” *Phys. Rev. Lett.*, vol. 98, pp. 021101, Jan 2007.

[49] M. Masuda and M. Sasaki, “Limits on nonstandard forces in the submicrometer range,” *Phys. Rev. Lett.*, vol. 102, pp. 171101, Apr 2009.

[50] R. S. Decca, D. López, H. B. Chan, E. Fischbach, D. E. Krause, and C. R. Jamell, “Constraining new forces in the casimir regime using the isoelectronic technique,” *Phys. Rev. Lett.*, vol. 94, pp. 240401, Jun 2005.

[51] R. S. Decca, D. López, E. Fischbach, G. L. Klimchitskaya, D. E. Krause, and V. M. Mostepanenko, “Tests of new physics from precise measurements of the casimir pressure between two gold-coated plates,” *Phys. Rev. D*, vol. 75, pp. 077101, Apr 2007.

[52] J. Chiaverini, S. J. Smullin, A. A. Geraci, D. M. Weld, and A. Kapitulnik, "New experimental constraints on non-newtonian forces below 100 micrometers," *Phys. Rev. Lett.*, vol. 90, pp. 151101, Apr 2003.

[53] Andrew A. Geraci, Sylvia J. Smullin, David M. Weld, John Chiaverini, and Aharon Kapitulnik, "Improved constraints on non-newtonian forces at 10 microns," *Phys. Rev. D*, vol. 78, pp. 022002, Jul 2008.

[54] "Laser quantum: ventus 1064 product page," `http://www.laserquantum.com/products/detail.cfm?id=22`, Accessed: 2017-08-22.

[55] "Thorlabs - lbf254-050-c - n-bk7 best form lens, 1", f = 50 mm, arc: 1050-1700 nm," `https://www.thorlabs.com/thorproduct.cfm?partnumber=LBF254-050-C`, Accessed: 2017-08-22.

[56] Tongcang Li, *Fundamental tests of physics with optically trapped microspheres*, Ph.D. thesis, The University of Texas at Austin, Austin, Texas, May 2011.

[57] "Bangs laboratories, inc. .3 μm silica beads in an aqueous suspension," `http://www.bangslabs.com/products/ordering/list/SS02001`, Accessed: 2017-08-10.

[58] "Mci - programmable compact spin coater (max. 8000 rpm, 4 wafer max.) with 3 sets of vacuum chucks & complete accessories - vtc-100a," `http://www.mtixtl.com/ProgrammableCompactSpinCoater0-8000rpm4waferMax-VTC-100A.aspx`, Accessed: 2017-08-22.

[59] I. Lekavicius, "Towards investigating the casimir effect in a new regime," 2013, B.S. thesis.

[60] "Apc international ltd. piezo distributor," `https://www.americanpiezo.com/`, Accessed: 2017-08-10.

[61] M. Beck, "Overcoming stiction forces: Launching silica microspheres into an optical trap," 2012, B.S. thesis.

[62] "Thorlabs - al1225-c - 12.5 mm n-bk7 aspheric lens, f=25 mm, na=0.23, arc: 1050-1700 nm," `https://www.thorlabs.com/thorproduct.cfm?partnumber=AL1225-C`, Accessed: 2017-08-22.

[63] "Segmented type ingaas photodiode - hamamatsu photonics," `http://www.hamamatsu.com/jp/en/product/category/3100/4007/4002/4205/4109/index.html`, Accessed: 2017-08-23.

[64] "Opa4227 (active) high precision, low noise operational amplifiers," `http://www.ti.com/product/OPA4227`, Accessed: 2017-08-22.

[65] D. Zuro, "Measuring the motion of micro-scale objects using light," 2013, B.S. thesis.

[66] Markus Aspelmeyer, Tobias J. Kippenberg, and Florian Marquardt, "Cavity optomechanics," *Rev. Mod. Phys.*, vol. 86, pp. 1391–1452, Dec 2014.

[67] N. A. Fuchs, *The Mechanics of Aerosols*, Dover, 1926.

[68] R. Brckner, "Properties and structure of vitreous silica. i," *Journal of Non-Crystalline Solids*, vol. 5, no. 2, pp. 123 – 175, 1970.

[69] Yohai Roichman, Bo Sun, Allan Stolarski, and David G. Grier, "Influence of nonconservative optical forces on the dynamics of optically trapped colloidal spheres: The fountain of probability," *Phys. Rev. Lett.*, vol. 101, pp. 128301, Sep 2008.

[70] "Mephisto lasers - coherent," `https://www.coherent.com/lasers/main/mephisto-lasers`, Accessed: 2017-09-01.

[71] "Amo laser systems - vescent photonics," `http://www.vescent.com/products/d2-series/`, Accessed: 2017-09-01.

[72] Dana Z. Anderson, "Alignment of resonant optical cavities," *Appl. Opt.*, vol. 23, no. 17, pp. 2944–2949, Sep 1984.

[73] CVI Melles Griot, "Gaussian beam optics - cvi melles griot 2009 technical guide, vol. 2, issue 1," Tech. Rep., CVI Melles Griot, 2009.

[74] Eric D. Black, "An introduction to pounddreverhall laser frequency stabilization," *American Journal of Physics*, vol. 69, no. 1, pp. 79–87, 2001.

[75] "Thorlabs - fds100 - si photodiode, 10 ns rise time, 350 - 1100 nm, 3.6 mm x 3.6 mm active area," `https://www.thorlabs.com/thorproduct.cfm?partnumber=FDS100`, Accessed: 2017-09-01.

[76] David P. Atherton, *Sensitive force measurements with optically trapped microspheres in high vacuum*, Ph.D. thesis, The University of Nevada, Reno, Reno, Nevada, May 2015.

[77] "Thorlabs - fdga05 - ingaas photodiode, 2.5 ns rise time, 800-1700 nm, 0.5 mm active area," `https://www.thorlabs.com/thorproduct.cfm?partnumber=FDGA05`, Accessed: 2017-09-01.

[78] M. Karam, "Tunable diode laser absorption spectroscopy of oxygen," 2010, B.S. thesis.

[79] K. Casey, "Search for corrections to newtonian gravity: Controlling nanospheres in an optical cavity," 2017, McNair Report.

[80] J. B. Johnson, "Thermal agitation of electricity in conductors," *Phys. Rev.*, vol. 32, pp. 97–109, Jul 1928.

[81] D. Sarid, *Scanning Force Microscopy: With Applications to Electric, Magnetic, and Atomic Forces*, Oxford Series in Optical and Imaging Sciences. Oxford University Press, 1994.

[82] W. Schottky, "Small-shot effect and flicker effect," *Phys. Rev.*, vol. 28, pp. 74–103, Jul 1926.

[83] T. A. Savard, K. M. O'Hara, and J. E. Thomas, "Laser-noise-induced heating in far-off resonance optical traps," *Phys. Rev. A*, vol. 56, pp. R1095–R1098, Aug 1997.

[84] "Newport - ag-ls25," `https://www.newport.com/p/AG-LS25`, Accessed: 2017-08-23.

[85] "Thorlabs - polaris-k05t6 - polaris sm05-threaded 1/2" mirror mount, 3 hex adjusters with lock nuts, 2 retaining rings included," `https://www.thorlabs.com/thorproduct.cfm?partnumber=POLARIS-K05T6`, Accessed: 2017-08-23.

[86] "Microcontroller designs for atomic, molecular, and optical physics laboratories," `http://www.phys.uconn.edu/~eyler/microcontrollers/`, Accessed: 2017-09-01.

[87] "The engineering toolbox," `http://www.engineeringtoolbox.com/linear-expansion-coefficients-d_95.html`, Accessed: 2017-08-14.